J. Micropalaeontology, 40, 15–35, 2021
https://doi.org/10.5194/jm-40-15-2021

Journal of Micropalaeontology
Open Access

Last Glacial Maximum to Holocene paleoceanography of the northwestern Ross Sea inferred from sediment core geochemistry and micropaleontology at Hallett Ridge

Romana Melis[1], Lucilla Capotondi[2], Fiorenza Torricella[3], Patrizia Ferretti[4], Andrea Geniram[1], Jong Kuk Hong[5], Gerhard Kuhn[6], Boo-Keun Khim[7], Sookwan Kim[5], Elisa Malinverno[8], Kyu Cheul Yoo[5], and Ester Colizza[1]

[1]Dipartimento di Matematica e Geoscienze, Università di Trieste, Via E. Weiss 2, 34127 Trieste, Italy
[2]Consiglio Nazionale delle Ricerche–Istituto di Scienze Marine (CNR-ISMAR), Via Gobetti 101, 40129 Bologna, Italy
[3]Dipartimento di Scienze della Terra, Università di Pisa, Via Santa Maria 53, 56126 Pisa, Italy
[4]Dipartimento di Scienze Ambientali, Informatica e Statistica, Università Ca' Foscari, Via Torino 155, Mestre, 30172 Venice, Italy
[5]Korea Polar Research Institute, Incheon, 21990, South Korea
[6]Alfred-Wegener-Institut Helmholtz Zentrum für Polar- und Meeresforschung, Am Alten Hafen 26, 27568 Bremerhaven, Germany
[7]Department of Oceanography, Pusan National University, Busan, 46241, South Korea
[8]Dipartimento di Scienze dell'Ambiente e della Terra, Università di Milano-Bicocca, Piazza della Scienza 4, 20126 Milan, Italy

Correspondence: Lucilla Capotondi (lucilla.capotondi@bo.ismar.cnr.it)

Received: 15 September 2020 – Revised: 1 February 2021 – Accepted: 2 February 2021 – Published: 10 March 2021

Abstract. During the Late Pleistocene–Holocene, the Ross Sea Ice Shelf exhibited strong spatial variability in relation to the atmospheric and oceanographic climatic variations. Despite being thoroughly investigated, the timing of the ice sheet retreat from the outer continental shelf since the Last Glacial Maximum (LGM) still remains controversial, mainly due to a lack of sediment cores with a robust chronostratigraphy. For this reason, the recent recovery of sediments containing a continuous occurrence of calcareous foraminifera provides the important opportunity to create a reliable age model and document the early deglacial phase in particular. Here we present a multiproxy study from a sediment core collected at the Hallett Ridge (1800 m of depth), where significant occurrences of calcareous planktonic and benthic foraminifera allow us to document the first evidence of the deglaciation after the LGM at about 20.2 ka. Our results suggest that the co-occurrence of large *Neogloboquadrina pachyderma* tests and abundant juvenile forms reflects the beginning of open-water conditions and coverage of seasonal sea ice. Our multiproxy approach based on diatoms, silicoflagellates, carbon and oxygen stable isotopes on *N. pachyderma*, sediment texture, and geochemistry indicates that abrupt warming occurred at approximately 17.8 ka, followed by a period of increasing biological productivity. During the Holocene, the exclusive dominance of agglutinated benthic foraminifera suggests that dissolution was the main controlling factor on calcareous test accumulation and preservation. Diatoms and silicoflagellates show that ocean conditions were variable during the middle Holocene and the beginning of the Neoglacial period at around 4 ka. In the Neoglacial, an increase in sand content testifies to a strengthening of bottom-water currents, supported by an increase in the abundance of the tycopelagic fossil diatom *Paralia sulcata* transported from the coastal regions, while an increase in ice-rafted debris suggests more glacial transport by icebergs.

Published by Copernicus Publications on behalf of The Micropalaeontological Society.

1 Introduction

Ice shelves are very sensitive to climatic variations, with their dynamics being related to the atmospheric and ocean warming–cooling causing changes in the accumulation and discharge of upstream glacial ice. The Ross Sea Ice Shelf, the largest in Antarctica, has been investigated over recent decades as it drains parts of the two main ice sheets, the West Antarctic Ice Sheet (WAIS) and the East Antarctic Ice Sheet (EAIS), which extended toward the outer continental margin during the Last Glacial Maximum (LGM) (Anderson et al., 2014, 2018; Halberstadt et al., 2016; Simkins et al., 2017). Even though the time and mode of the retreat of these ice sheets since the LGM have been extensively studied and new models have recently been presented (e.g., Golledge et al., 2014; Lowry et al., 2019), some controversies still remain due to the difficulties in obtaining accurate radiocarbon dates. Published radiocarbon ages are predominantly based on acid-insoluble organic matter (AIOM) extracted from bulk sediments (Livingstone et al., 2012; Anderson et al., 2014; Prothro et al., 2020). Indeed, the ages obtained through these methods are frequently anomalously old, with an overestimated age of glacial retreat (e.g., Andrews et al., 1999; Hillenbrand et al., 2009; Anderson et al., 2014; Prothro et al., 2020). For this reason, the availability of well-preserved calcareous material represents an excellent opportunity to construct a more accurate age model as evidenced in investigations performed in the Ross Sea (Bart et al., 2018; Melis and Salvi, 2020; Prothro et al., 2020). In this work we investigate a sedimentary interval found in a deep-sea core at the Hallett Ridge (northwestern Ross Sea) characterized by the presence of rich and well-preserved calcareous foraminiferal assemblages. The recovery of sediments containing foraminifera in the Antarctic continental margin represents a good opportunity for paleoenvironmental studies lacking the continuous presence of biogenic calcium carbonate. In the Southern Ocean, the occurrence of foraminifera is strongly controlled by water-mass characteristics, which determine the solubility of $CaCO_3$ on the seafloor (e.g., Murray and Pudsey, 2004; Hauck et al., 2012; Dejong et al., 2015). However, their occurrence and distribution are very useful to characterize the lithofacies associated with glacial retreat patterns (e.g., Bart et al., 2016; Majewski et al., 2018; Prothro et al., 2018, 2020). In this study, using integrated proxies, we provide new information on paleoceanographic conditions in order to reconstruct the paleoenvironmental changes in the Hallett Ridge area since Marine Isotope Stage (MIS) 2. Our results, including benthic foraminifera, diatoms, and silicoflagellates, are used to better define paleoenvironmental and paleoceanographic conditions. These microfossil groups are well-known as useful proxies for reconstructing the paleoenvironmental settings recorded in the sedimentary sequence deposited in diverse facies related to an ice shelf–sheet from sub-glacial to open marine conditions (e.g., Smith et al., 2019, and references herein).

Ross Sea ice sheet–shelf dynamics were principally investigated in the continental shelf via geophysical and geological methods (Domack et al., 1999; Anderson et al., 2014; Prothro et al., 2018, 2020; Smith et al., 2019). The typical sedimentary succession from sub-glacial diamicton toward proximal to distal deglacial glaciomarine sediments and Holocene open marine diatom-bearing mud, recording a progressive retreat of the ice sheet–shelf and the final onset of seasonal open marine conditions, has been well-documented (Prothro et al., 2018, 2020; Smith et al., 2019). In this study we extend the investigations to the outer continental shelf–slope system, which is more complex and still scarcely investigated (Quaia and Cespuglio, 2000; Bonaccorsi et al., 2007; Tolotti et al., 2013; Frank et al., 2014). The sedimentation of the continental slopes is strongly influenced by the dominant oceanographic processes and, in some cases, by the downward transport of sediment through the gravitational sediment flow, which includes collapse, turbidity, and debris flows (Jacobs, 1989). Moreover, based on the radiocarbon dating performed on *Neogloboquadrina pachyderma*, we try to link and test models of the glacial retreat history.

2 Study area

The Hallett Ridge is a structural high bordering the west side of the Central Basin, a semi-closed basin located at the mouth of the JOIDES Basin at the continental shelf break of the western Ross Sea (Fig. 1a). The multibeam bathymetry acquired during the IBRV *Araon* expeditions ANA03B in 2013 and ANA05B in 2015 (Fig. 1b) shows some slope failures and bathymetric ridges that are contour-parallel elongated along the eastern slope of Hallett Ridge (Kim, 2018). The simultaneously acquired sub-bottom profiler (SBP) data show that acoustically stratified facies developed in the slope failure area (Fig. 1c), while relatively weak subsurface reflections are observed below high-amplitude seafloor reflection on the contour-parallel mounds of the eastern slope of Hallett Ridge (Kim, 2018). This provides indirect evidence that less compacted and/or finer-grained sediment in the slope failure area is relatively thicker than the bathymetric highs.

The studied area is influenced by dense and salty High-Salinity Shelf Water (HSSW) coming from the mouth of the JOIDES Basin. This water mass exported from the continental shelf mixes with Circumpolar Deep Water (CDW) as it descends the continental slope, producing Antarctic Bottom Water (AABW) (Budillon et al., 2011; Castagno et al., 2019). AABW plays a key role in the thermohaline circulation in the global climate system (Jacobs, 2004; Colleoni et al., 2018; Tinto et al., 2019). On the other hand, the Central Basin represents one of the preferred pathways for warm CDW flowing onto the continental shelf (Dinniman et al., 2011) as modified CDW (mCDW) providing the main source of heat and nutrients (Smith et al., 2012; Stevens et al., 2020) to the Ross Sea continental shelf. Considering that this area has been most af-

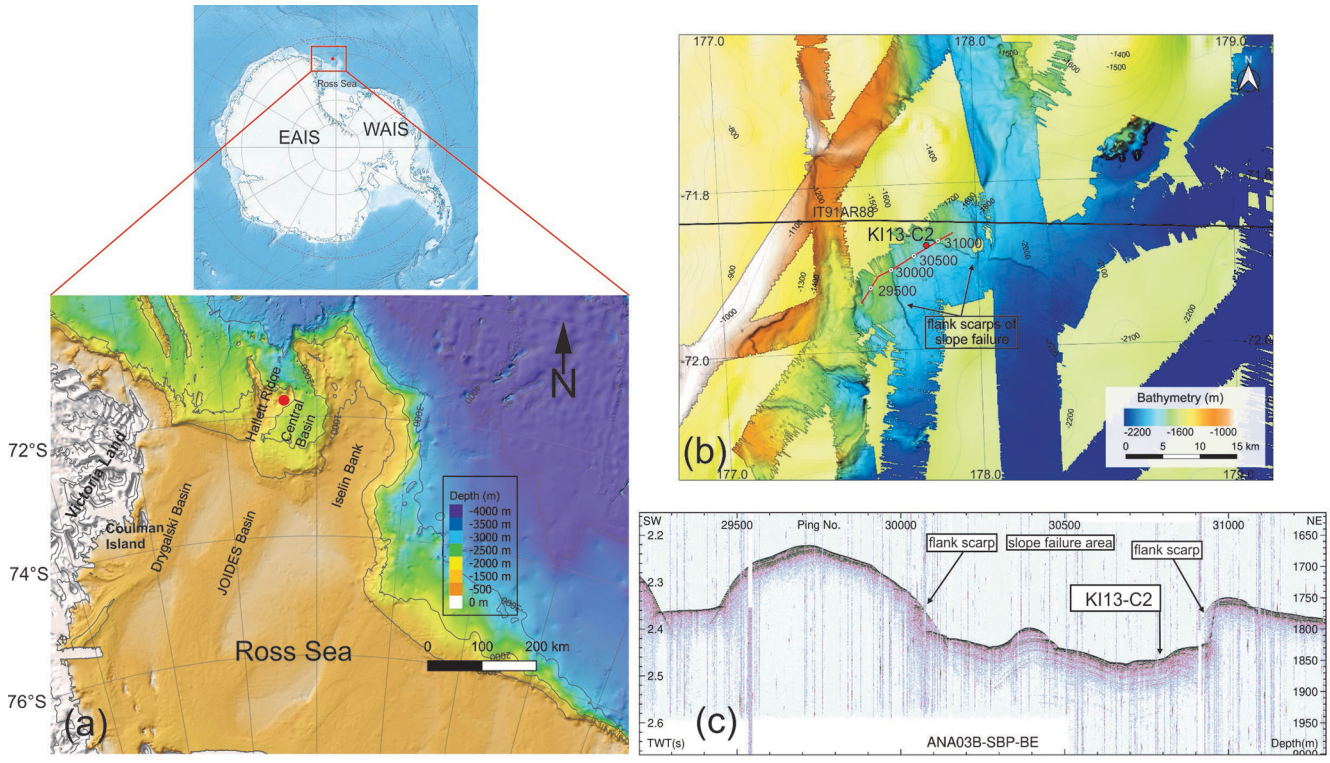

Figure 1. **(a)** Bathymetric map of the northwestern Ross Sea (modified from Arndt et al., 2013) and location of the KI13-C2 core (red dot). **(b)** Multibeam bathymetry imagery of the study area and core location. The black line indicates the multi-channel seismic (MCS) line IT91AR88. The red line and white dots represent the sub-bottom profile (SBP) data of ANA03B-SBP-BE, and labels refer to intervals of 500 ping numbers illustrated in the **(c)** SBP of ANA03B-SBP-BE and the core location. The Antarctica relief location map is from Wikimedia Commons contributors.

fected by the contributions of the EAIS (Farmer et al., 2006; Anderson et al., 2014), the sedimentary sequences preserved in the Central Basin are located in an ideal location to provide important information about the HSSW dynamics and the EAIS evolution during the Quaternary glacial and interglacial cycles.

3 Material and methods

Gravity core KI13-C2 (71°52.5′ S, 177°48.1′ E; water depth ∼ 1800 m) was collected during the IBRV *Araon* expedition in February 2013 in the framework of a joint project between Italian and Korean researchers (PNRA/ROSSLOPE and K-PORT Projects). The core (232 cm long) is located in the northwestern side of the Central Basin near the right flank of the Hallett Ridge. Based on the SBP and multibeam data acquired during the ANA03B expedition, the core was collected in the trough between the small contour-parallel mounds (Fig. 1c), indicating that this area was affected by along-slope bottom current activity. Here we report data from the upper 60 cm of sedimentary interval in which an abundant presence of calcareous foraminifers has been recorded.

3.1 Sedimentary analyses

For grain size analyses, 17 samples were treated with hydrogen peroxide to remove organic matter and sieved to separate the < 2 mm fraction. Carbonate was removed with acetic acid in all samples with carbonate content > 5 %, in agreement with McCave et al. (1995). The grain size of the < 2 mm size fraction was determined using the Malvern Mastersizer Hydro2000S diffraction laser particle size analyzer from the Department of Mathematics and Geosciences, Trieste. Sand and mud classes were determined using the Friedman and Sanders (1978) grain size classification. Grain size parameters were calculated using the Folk and Ward formulas (Folk and Ward, 1957). The > 2 mm fraction was counted separately.

3.2 Chronology

The chronology of the studied core is based on nine accelerator mass spectrometry (AMS) radiocarbon dates obtained at the Poznań Radiocarbon Laboratory located at Adam Mickiewicz University (Poland) and with the MICADAS (Wacker et al., 2013) at the Alfred-Wegener-Institut Helmholtz-Zentrum für Polar- und Meeresforschung (AWI,

Germany). Five radiocarbon analyses were made using acid-insoluble organic matter (AIOM), and four were carried out on *N. pachyderma* tests (Table 1).

Considering the different carbonate and organic carbon matrices, we decided to directly calibrate the carbonate dates and to treat AIOM dates prior to the calibration of ^{14}C ages. Radiocarbon chronologies using the AIOM fraction from bulk sediments are often compromised by contamination from reworked ancient organic carbon derived from glacial erosion and/or from the reworking of unconsolidated sediments (see Mezgec et al., 2017; Tesi et al., 2020, for a discussion). This is evidenced by AIOM dates of Antarctic surface sediments that extend over several thousand years (Andrews et al., 1999; Pudsey et al., 2006).

The down-core AIOM dates were corrected by the AIOM age of the preserved core-top sediments of the box core KI13-BC3, which was collected at the same site. We assumed that the age difference between the AIOM ^{14}C age of the box-core and core-top sediment, along with the marine reservoir effect (MRE), represents local contamination with older organic matter in this area, and hereafter it is referred to as "local contamination offset" (LCO; see the discussion in Hillenbrand et al., 2009). Before calibrating the ^{14}C dates, the LCO obtained for this area was subtracted from the AIOM ^{14}C down-core ages (LCO-corrected ages), assuming that both MRE and LCO did not change over the Holocene (see Hall et al., 2010; Mezgec et al., 2017, for details). We used an MRE of 1.1 ± 0.12 ka ^{14}C suggested by Hall et al. (2010) for the Ross Sea area carbonate samples.

The LCO-corrected AMS ^{14}C dates obtained for AIOM and *N. pachyderma* tests were converted into calibrated ages by means of Clam 2.3.2 (Blaauw, 2010) at 95 % confidence ranges. The Marine13 calibration curve (Reimer et al., 2013), assuming a regional marine offset (ΔR) of 0.79 ± 0.12 ka from the global MRE (Hall et al., 2010), was used. CLAM 2.3.2 (Blaauw, 2010) was also used to calculate the age–depth model through a linear interpolation function between dated levels with 1000 iterations (Fig. 2). Uncorrected and calibrated ^{14}C data are summarized in Table 1; all the ages reported in this paper represent the calibrated ages unless otherwise specified.

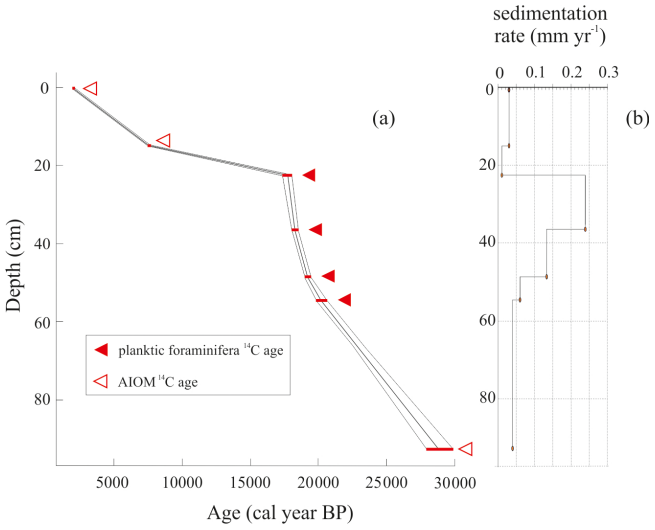

Figure 2. **(a)** Age–depth model based on the linear interpolation of best point calibration ages from AMS ^{14}C dates obtained using Clam software (Blaauw, 2010). The dotted lines show the 95 % confidence intervals based on 1000 iterations. **(b)** Sedimentation rate in millimeters per year.

3.3 Geochemical analyses

3.3.1 Sediment geochemistry

Total inorganic carbon (TIC) content was measured on 33 levels every 2 cm using a UIC CO_2 coulometer (model CM5014) at Pusan National University (Korea). TIC content was used to calculate the $CaCO_3$ content as a weighted percentage by the multiplication of factor 8.333 ($CaCO_3$ / C ratio). The analytical precision of $CaCO_3$ content as a relative standard deviation is ± 1 %. The total carbon (TC) content of the same sediment samples was measured by Flash 2000 Series elemental analyzer. The analytical precision of TC is less than ± 0.1 %. TOC content was calculated by the difference between TC and TIC.

3.3.2 Stable oxygen and carbon isotopes on planktic foraminifera

Stable oxygen and carbon isotope measurements were carried out at 1 cm resolution on 39 samples (from 18 to 56 cm) using the planktic foraminifera *Neogloboquadrina pachyderma*. At least 20 adult specimens picked from the > 250 µm sediment size fraction were used for the analysis in order to provide significant carbon dioxide. Specimens were lightly crushed and soaked in 1 % hydrogen peroxide for 30 min in individual vials in order to remove any possible organic contaminant. Analytical-grade acetone was then added, and samples were cleaned ultrasonically for 30 s to remove fine-grained particles, after which the excess liquid and residue were siphoned off. Samples were finally oven-dried overnight at 50 °C before the analysis. Stable isotope analyses were carried out on VG SIRA mass spectrometer coupled with a Micromass Multicarb sample preparation system and a Thermo Finnigan MAT253 mass spectrometer fitted with a Kiel device. Measurements of δ^{18}O and δ^{13}C were determined relative to the Vienna Peedee Belemnite (VPDB) standard, and the analytical precision was better than 0.08 ‰ for δ^{18}O and 0.06 ‰ for δ^{13}C. All isotope measurements were performed at the Godwin Laboratory for Palaeoclimate Research, Department of Earth Sciences, University of Cambridge (UK).

Table 1. AMS ^{14}C ages with calibrated calendar ages $\pm 2\sigma$ (years) as well as applied local contamination offset and reservoir age correction (see text) of the studied core. The calendar ages were calibrated using the Clam 2.3.2 software with a Marine13 calibration curve (Reimer et al., 2013). A constant reservoir correction of 1144 ± 121 years with a ΔR of 791 ± 121 years (Hall et al., 2010) was applied. Calibrated age ranges are at 95 % confidence.

Core and box core ID	Sample depth (cm)	Carbon source[b]	Lab no.[c]	Conventional ^{14}C age (yr BP)	Error (years)	LCO[d]	LCO corr. age (yr BP)	Median probability cal age (yr BP)	Lower cal range (yr BP)	Upper cal range (yr BP)	Sedim. rate (mm yr^{-1})
KI13-BC3[a]	0–1	AIOM	Poz-69634	5050	40						
KI13-C2	0–1	AIOM	Poz no. 2-69635	7110	40	3950	3160	1998	1887	2108	–
KI13-C2	14–15	AIOM	Poz no. 2-69636	11 780	80	3950	7830	7535	7404	7666	0.03
KI13-C2	22–23	*N. pachy*	AWI-4812.1.1	15 710	143	–	–	17 669	17 317	18 020	0.01
KI13-C2	36–37	*N. pachy*	Poz-75519	16 230	100	–	–	18 262	17 995	18 528	0.24
KI13-C2	48–49	*N. pachy*	Poz no. 2-75519	17 080	90	–	–	19 179	18 926	19432	0.13
KI13-C2	54–55	*N. pachy*	AWI-4813.1.1	17 930	166	–	–	20 188	19 775	20 601	0.06
KI13-C2	92–93	AIOM	Poz-121684	29 900	450	3950	25 950	28 856	27 879	29 833	0.04

[a] Box core. [b] AIOM: acid-insoluble organic matter; *N.pachy*: monospecific planktonic tests. [c] Poz: Poznań Radiocarbon Laboratory, Poland; AWI: Alfred-Wegener-Institut Helmholtz-Zentrum für Polar- und Meeresforschung, Germany. [d] LCO: local contamination offset; see text for explanation.

3.4 Micropaleontological analyses

3.4.1 Foraminifera

A total of 22 sediment samples (1 cm thick) collected on average every 1, 2, and 4 cm, depending on the sedimentation rate, were investigated for foraminiferal analysis. The samples were dried, weighed, and wet-sieved on a 63 µm mesh. The whole fraction > 63 µm was investigated. In the carbonate-rich interval, the samples were split in order to obtain an aliquot containing approximately 300 planktic and benthic individuals. The density for both planktic and benthic foraminifera was expressed as the number of specimens per gram of total dry sediment, hereinafter referred to as specimens per gram.

Following the ecology requirements of *N. pachyderma*, we differentiated between encrusted (adults) and non-encrusted (juveniles) specimens as the two different morphologies record different depth habitats and seasons (Mikis et al., 2019). In detail, encrusted specimens dominate during austral spring and summer seasons; conversely, smaller and non-encrusted specimens characterize autumn and winter conditions. The density of *N. pachyderma* was reported separately for encrusted and non-encrusted specimens. Foraminiferal benthic counts were performed considering only well-preserved specimens, and data were reported as relative abundance and as densities (the number of specimens per gram of total sediment). All foraminifera were identified at species levels, except for unilocular forms (*Fissurina*, *Lagena*, and *Oolina*) and small Discorbidae, which were identified at the generic level (Table S1 in the Supplement). The identification mainly follows Violanti (1996), Igarashi et al. (2001), Murray and Pudsey (2004), Majewski (2005), and Majewski et al. (2018). The Ellis and Messina online catalog of foraminifera (http://www.micropress.org/, last access: 1 September 2020) was consulted for original taxa descriptions. The number of broken and/or etched foraminifera allowed us to calculate the percent of fragmentation for each level.

3.4.2 Diatoms

A total of 33 samples collected on average every 1, 2, and 4 cm, depending on the sedimentation rate, were obtained for diatom analyses. Diatom slide preparation followed the technique described by Rathburn et al. (1997). Diatom analysis was performed with a light microscope at 1000× magnification; Zeiss (Immersol oil 518) immersion oil was used to allow the observation. At least 300 diatom valves in each sample were identified and counted following the counting method outlined by Crosta and Koç (2007). The relative abundance was determined for each taxon as the ratio between the diatom species and the total diatom abundance. Species occurring at < 2 % were not considered statistically significant (Taylor and Sjunneskog, 2002). The total absolute diatom abundance (ADA) in terms of the number of valves per gram of dry weight (v gdw^{-1}) was determined using the formula described by Armand (1997).

3.4.3 Silicoflagellates

Diatom slides were scanned for silicoflagellates at 200× magnification using an Olympus BX50 light microscope. When possible, 50–60 specimens of *Stephanocha speculum* were counted in each sample to calculate the absolute silicoflagellate abundance (ASA) in terms of silicoflagellates per gram of dry weight (s gdw^{-1}) following the formula used for diatoms. A slide surface up to 250 mm^2 was scanned when silicoflagellate abundance was scarce, resulting in a minimum detectability of 2×10^3 s gdw^{-1}. Each specimen of *S. speculum* was observed at 1000× with immersion oil for a detailed identification of the different morphotypes, follow-

ing the taxonomic concepts of Malinverno (2010) and the recent review of Jordan and McCartney (2015). Morphotypes were grouped according to their ecological preferences (Malinverno et al., 2016), and their relative abundances (% values) were calculated only where silicoflagellate density was well above the detection limit, which is from the top to the depth of 33 cm.

4 Results

4.1 Chronology

All obtained radiocarbon ages are consistent with their stratigraphic position, and therefore any effect of sediment reworking was likely negligible. The chronological reconstruction based on the calibrated ages corresponds to the time interval from the late MIS 2 to the late Holocene (22.6–2.2 ka) including the LGM (i.e., 26.5–19 ka; sensu Clark et al., 2009). Considering that the chronology of the interval 20.2–18.0 ka was obtained using well-preserved calcareous foraminifera, we are confident that the age model for this period is reliable, whereas the age model determined using the AIOM could be less accurate due to the well-known problems related to the aging of organic matter (e.g., Andrews et al., 1999; Hillenbrand et al., 2009) (Fig. 2). The sedimentation rate, calculated using the dated levels, increases between 20.2 and 18.3 ka (from 0.06 to 0.24 mm yr^{-1}) and subsequently decreases toward the core top, from 0.24 to 0.03 mm yr^{-1}, with the lowest sedimentation rate of 0.01 mm yr^{-1} between 17.7 and 7.5 ka (Table 1).

4.2 Sediment grain size

The sediment at the base of the investigated core interval (below 60 cm, sediment older than 20 ka) is characterized by dark gray silty sand with a high sand content (up to 75 %). The mean diameter (M_z) of these oldest sediments corresponds to a fine sand (average M_z 3.9 Φ) (Fig. 3). The sediment gradually changes from dark gray to olive brown sandy silt toward the top core, where weak dark millimeter-thick laminae are present. The average of the M_z is 5.2 Φ (fine silt) with ca. 25 %–30 % sand, 60 %–70 % silt, and 3 %–8 % clay from 20.0 to 18.3 ka. Sand content reaches a high value (42 %) at around 18 ka and at the core top. The minimum values of sand (14 %–20 %) are recorded between 17.7 and 10.0 ka. The gravel fraction from granules to pebbles is always present, is more concentrated at the base of the studied interval until 18.3 ka, and tends to be scattered upward (Fig. 3).

4.3 Geochemical results

4.3.1 Paleoproductivity proxies

The TOC content ranges from 0.03 % to 0.5 %; the values gradually increase from 20.7 (0.04 %) to 17.7 ka (until 0.5 %) and decrease in the upper part of the investigated interval (< 0.2 %) (Fig. 3). $CaCO_3$ content displays values from 0.6 % to 10.5 % (mean value 4.3 %); the variations are consistent with the presence of foraminifera, and the maximum value of $CaCO_3$ is observed at 18.0 ka (Figs. 3 and 4). The molar ratio C_{org}/N_{tot} (mean value 7.1) is characterized by values from a minimum of 5.1 (at 18.0 ka) to a maximum of 8.8 (at 17.7 ka) (Fig. 3). Its variation is in agreement with the TOC distribution.

4.3.2 Stable isotope results

Stable oxygen ($\delta^{18}O$) and carbon ($\delta^{13}C$) isotope ratios were measured on the planktic foraminifera *Neogloboquadrina pachyderma* between 20.5 and 11.6 ka (Fig. 4). The $\delta^{18}O$ values range from 4.7 ‰ to 5.3 ‰ (Supplement); the $\delta^{18}O$ record increases at 19.1 ka towards a maximum value of 5.3 ‰ at 18.7 ka and remains relatively high until 18.1 ka. Following this event, *N. pachyderma* $\delta^{18}O$ reveals a plateau of reduced-amplitude variability from 18.1 to 17.7 ka, with values lower than 5.0 ‰ (Fig. 4). The $\delta^{13}C$ values range from −0.1 ‰ to 0.4 ‰ (Supplement). The $\delta^{13}C$ record documents a generally increasing trend from the bottom of the sequence (0 ‰ at 20.5 ka) up to 17.8 ka, when it reaches a maximum value of 0.4 ‰, followed by decreasing $\delta^{13}C$ values to a minimum of 0 ‰ at 15.6 ka (albeit defined by a single data point) before a moderate to minimal rise to 0.12 ‰ by 11.6 ka (Fig. 4).

4.4 Micropaleontological content

4.4.1 Foraminiferal assemblage

Neogloboquadrina pachyderma (juveniles and adults) is the only planktic species present. It is abundant from 19.8 to 17.7 ka, in which it marks the maximum occurrence, varying from 173 to 1915 specimens per gram at 18.3 ka (Fig. 4). Tests of *N. pachyderma*, both juveniles and adults, are generally well-preserved with little to no evidence of reworking. This species is absent during the Holocene except at around 3.7 ka, in which very few tests are recovered.

A total of 31 benthic species, representing 27 genera, were identified (Table S1). Several broken and damaged tests were observed at around 23–20 ka (fragmentation > 50 %), but well-preserved specimens dominate the rest of the studied interval, except for the sediments younger than 12.0 ka, for which increasing dissolution was evident (Fig. 4). The benthic foraminifera (abundance varying from 1 to 3253 specimens per gram, average 453 specimens per gram) are more abundant than the planktic ones (varying from 1 to

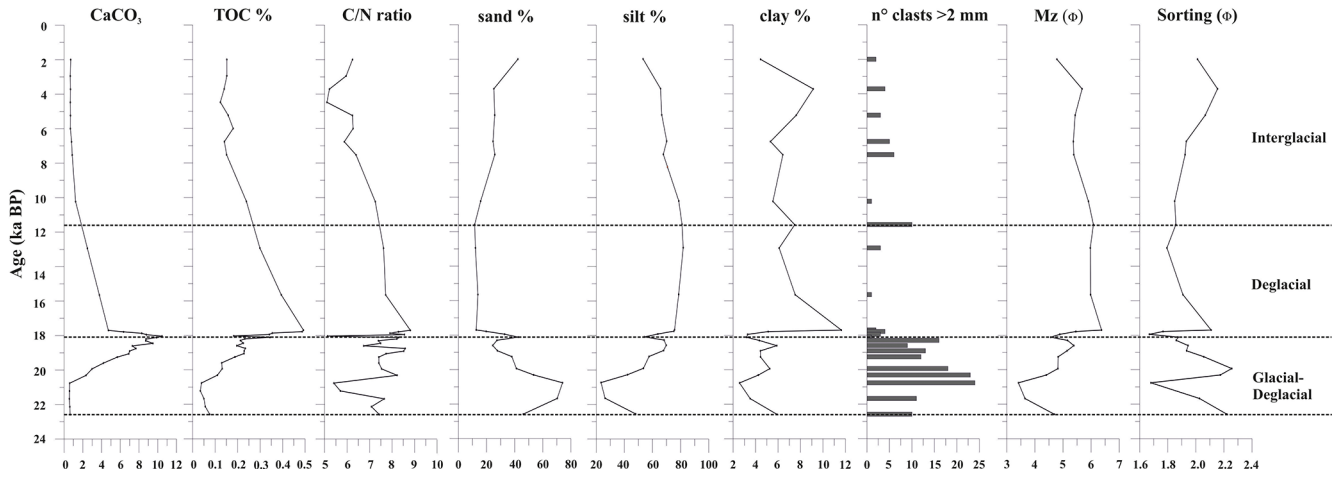

Figure 3. Sediment geochemistry and texture of the studied core. From left to right: down-core distribution of $CaCO_3$ (%), organic carbon (%), C_{org}/N_{tot} content, sand (%), silt (%), clay (%), number of clasts > 2 mm in size, mean diameter (M_z), and sorting in Φ. The top level of this core dates to 2.0 ka.

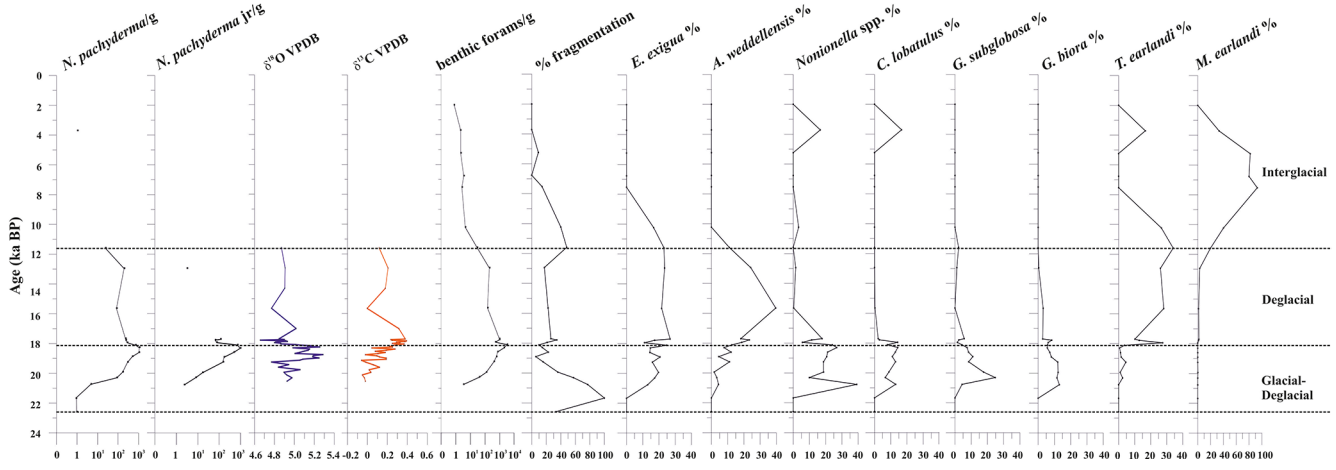

Figure 4. From left to right: down-core distribution of planktic (adult and juvenile forms) *N. pachyderma* (as the number of specimens per gram of dry sediment in logarithmic scale), stable oxygen and carbon isotopes on *N. pachyderma*, abundance (as the number of specimens per gram of dry sediment, logarithmic scale) of benthic foraminifera, fragmentation (%), and relative abundance (%) of benthic foraminifera. The top level of this core dates to 2.0 ka.

1915 specimens per gram, average 327 specimens per gram). Overall, the benthic foraminifera density is high from 19.9 to 18.1 ka (from 123 to 3253 specimens per gram, respectively) and then declines rapidly especially from 11.6 to 2.0 ka (from 203 to 0.8 specimens per gram, respectively) (Fig. 4). The benthic taxa are always present throughout the studied interval, except at 21.7 ka (Fig. 4). The most abundant species are *Epistominella exigua* (mean value 12.8 %), *Trifarina earlandi* (9.0 %), *Globocassidulina biora* (8.9 %), *Alabaminella weddellensis* (8.7 %), *Nonionella iridea* (7.8 %), *Cibicides lobatulus* (5.6 %), *Globocassidulina subglobosa* (4.5 %), and *Nonionella bradyi* (2.9 %) (Table S1). Agglutinated taxa, mainly represented by *Miliammina earlandi*, are rare and mainly occur during the Holocene. *Epistominella exigua* and *A. weddellensis* characterize the assemblage until about 10.0 ka. *Trifarina earlandi* is frequently observed from 18.0 to 11.3 ka and declines upward. *Cibicides* spp., *Globocassidulina* spp., and *Nonionella* spp. dominate at the base of the calcareous interval.

4.4.2 Diatom assemblage

A total of 34 genera and 44 species of diatoms are found in the studied samples. The diatoms are generally well-preserved and do not show the typical dissolution characteristics commonly represented by the loss of the valve margin and/or the breakage of the middle part. Furthermore, considering the higher presence of *Fragilariopsis kerguelensis* than *Thalassiosira lentiginosa* (Table S2) and in agreement with

Crosta and Koç (2007), the dissolution effect is believed to be absent or very limited.

The diatom assemblage is mainly characterized by *Actinocyclus actinochilus, Eucampia antarctica* var. *recta, Fragilariopsis curta, Fragilariopsis obliquecostata, F. kerguelensis, Thalassiosira antarctica*, and *Chaetoceros* resting spores (CRS) (Table S2). The diatom concentration (ADA) varies from 2.71 to 242×10^6 v gdw^{-1} with increasing values until 17.7 ka, when it reaches its maximum value, followed by a decreasing trend toward the core top, where the ADA value is 2.72×10^6 v gdw^{-1} (Fig. 5). CRS is the dominant species (average 36.3 %), with values up to 60 %. *E. antarctica*, *F. obliquecostata*, and *T. antarctica* dominate the diatom assemblage at the base of the studied interval from 23.0 to approximately 18.0 ka. Specifically, *F. obliquecostata* and *T. antarctica* have the same frequency trend, with the highest value (18.6 % for *F. obliquecostata* and 20.9 % for *T. antarctica*) at around 20.0 ka. *Eucampia antarctica* increases from 20.8 to 18.3 ka (from 19.0 % to 46.5 %), when it reaches its maximum value. From this interval toward the top core it decreases. From about 18.1 to 11.6 ka, *F. kerguelensis* dominates the diatom assemblage (value varies from 14.9 % to 33.8 % at 17.7 ka), showing a decrease at around 10 ka and from about 4 ka toward the top. From 3.3 to 2.6 ka, *F. obliquecostata*, together with *F. curta*, reaches its maximum frequency (Fig. 5).

4.4.3 Silicoflagellate assemblage

Stephanocha speculum is the only silicoflagellate species observed in the core sediments. Its concentration (ASA) is low and sparse from 22.6 to 18.3 ka, and it then increases to 1–5 $\times 10^5$ skeletons gdw^{-1} from 18.1 ka to the Holocene, reaching peak values of 2–4 $\times 10^6$ skeletons gdw^{-1} at around 5.2–4.5 ka (Fig. 5). Within this species, the dominant varieties are represented by *S. speculum* var. *monospicata* and var. *bispicata* (Table S2). Their cumulative values, plotted along with var. *speculum*, are usually > 50 % throughout the core, excluding lower values at around 18.0, 10.2, and 3.3–2.0 ka (Fig. 5). At these times, there is an increase in *S. speculum* var. *coronata* (individuals with a complete or almost complete crown of apical spines). Rare varieties include *S. speculum* var. *minuta*, and var. *binocula*, as well as individuals with three to four apical spines or with cannopilid apical structure, pentagonal, heptagonal, and aberrant morphologies (Table S2).

5 Discussion

The investigated sedimentary sequence corresponds to the time interval from the late MIS 2 to the late Holocene (22.6–2.0 ka). Results obtained from the multiproxy study allow us to identify three time intervals: 22.6–18.1 ka, 18.1–11.6 ka, and 11.6–2.0 ka in which significant micropaleontological, sedimentological, and geochemical changes occurred (Fig. 6). These times intervals will be referred to in the text as the glacial–deglacial transition, the deglacial period, and the interglacial period, respectively.

5.1 Glacial–deglacial transition (time interval 22.6–18.1 ka)

5.1.1 Interval 22.6–20.8

During the LGM, highly expanded ice sheets grounding below the sea level extended across the continental shelf of the Ross Sea, approximately reaching Coulman Island in the western sector (Licht et al., 1996; Shipp et al., 1999; Anderson et al., 2002; Bentley et al., 2014; Prothro et al., 2020). While the extension of the ice sheets (marine grounded ice) is quite well-known (e.g., Livingstone et al., 2012; Anderson et al., 2014; Mackintosh et al., 2014), there is a lack of data about the exact extension of the ice shelf in this region. Prothro et al. (2020) proposed a reconstruction of the ice shelf extension in the northwestern Ross Sea starting from 20 ka, mainly considering the data coming from Melis et al. (2002), Melis and Salvi (2009), and Mezgec et al. (2017). However, the Hallett Ridge region is still under investigation.

In the studied core, from 22.6 to 20.8 ka, the foraminifera are very scarce and often highly damaged. They are represented by the planktic *N. pachyderma* and some benthic genera such as *Cibicides*, *Epistominella,* and *Nonionella* (Fig. 4). In this period the diatom content is low, but the high abundance of CRS and dominance of *E. antarctica* var. *recta*, which usually represents conditions of relative iron enrichment, suggest iceberg melting conditions (Fig. 5, Table 2). Also, the high gravel and sand fraction contents, mainly derived from ice-rafted debris (IRD), suggest strong glacial influence, like the proximity of the ice shelf calving zone, where the sedimentation was dominated by terrigenous sediments (McGlannan et al., 2017; Smith et al., 2019). We cannot exclude the possibility of a certain amount of sediment contribution from the slope failure at the core site. Although the low preservation and scarcity of foraminifera could be interpreted as proximity to the grounding line, as suggested by Bart et al. (2016) and Majewski et al. (2020), it is well-known that neither the ice sheet nor the ice shelf reached the continental shelf margin during the LGM (e.g., Prothro et al., 2018, 2020). Overall, the sedimentological (i.e., high IRD content) and geochemical (high C / N ratio) conditions, along with the low diatom content, indicate the proximity of the calving zone, in agreement Smith et al. (2019), and the beginning of the ice shelf destabilization (Fig. 6). Possible proximity to an ice shelf has also been proposed for this area by Tolotti et al. (2013) and Kim et al. (2020).

5.1.2 Interval 20.8–18.1

The time interval from 20.8 to 18.1 ka is characterized by the peak in abundance of *N. pachyderma*, with adults and juvenile forms (with a comparable abundance up to 1000 spec-

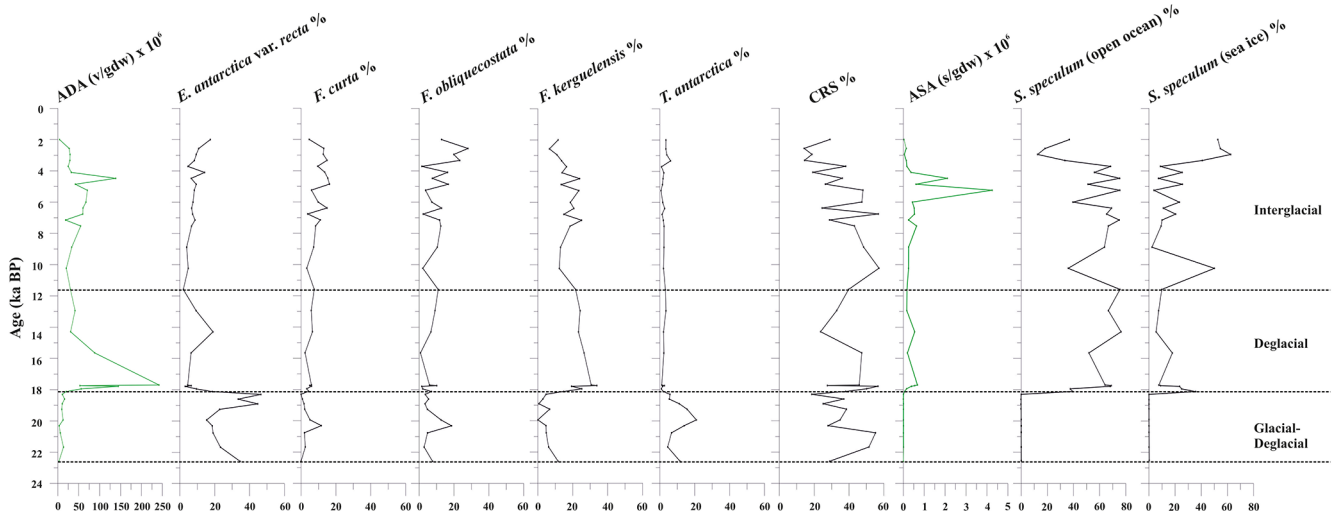

Figure 5. From left to right: absolute diatom abundance (ADA), down-core distribution of diatoms (%), absolute silicoflagellate abundance (ASA), and down-core distribution of *Stephanocha speculum* varieties. *S. speculum* (open ocean) includes *S. speculum* var. *monospicata*, var. *bispicata*, and var. *speculum,* while *S. speculum* (sea ice) includes *S. speculum* var. *coronata*. The top level of this core dates to 2.0 ka.

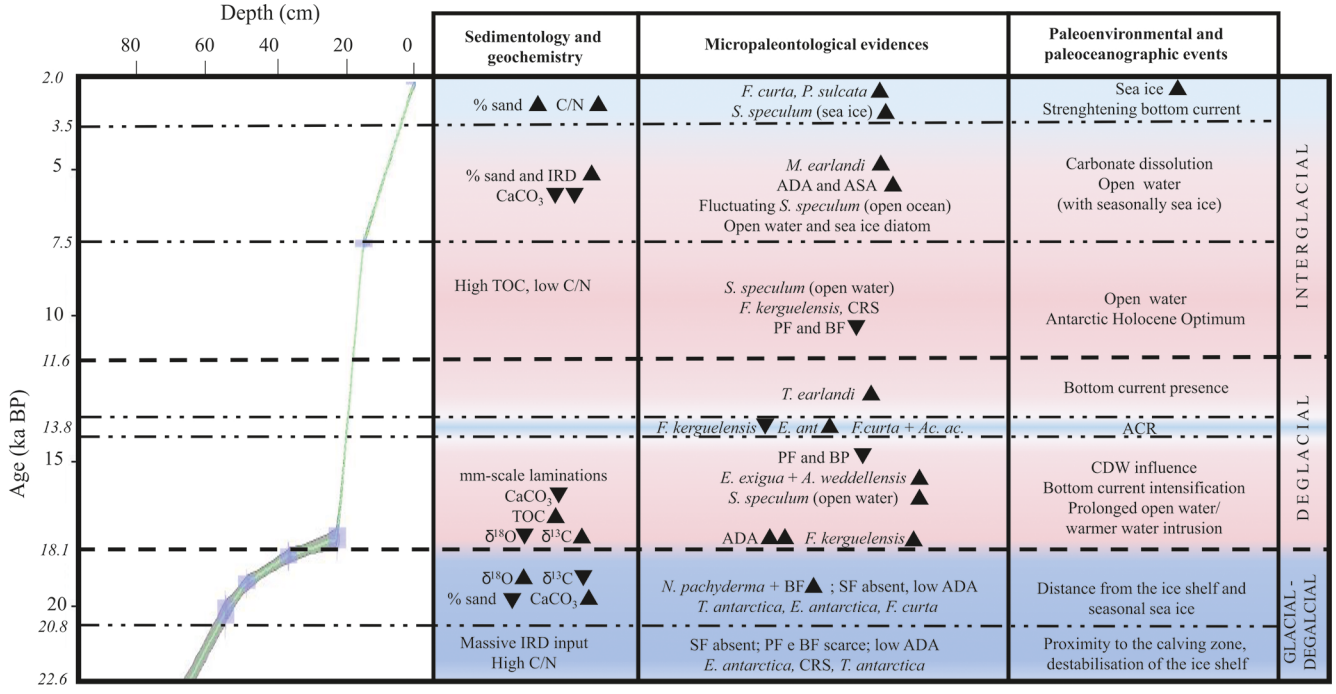

Figure 6. Age–depth plot for core KI13-C2 in the investigated interval. The main paleoenvironmental changes are illustrated, supported by geochemical, chemical, sedimentological, and micropaleontological data. The blue areas represent colder periods, and the pink areas represent warmer periods. Bold horizontal dashed lines are visual divisions between the three intervals discussed in the text; dotted lines highlight the main paleoenvironmental phases. Black triangles indicate increasing or decreasing relative occurrences of species. IRD: ice-rafted debris; TOC: total organic carbon; C/N: carbon / nitrogen ratio; ADA and ASA: diatom and silicoflagellate concentration, respectively; CRS: *Chaetoceros* resting spore; SF: silicoflagellates; PF: planktic foraminifera; BF: benthic foraminifera; ACR: Antarctic Cold Reversal; CDW: Circumpolar Deep Water.

Table 2. Taxonomy and ecology of the most abundant diatoms, silicoflagellates, and planktic and benthic foraminiferal species identified in the studied core.

	Ecology	References
Diatom species		
Actinocyclus actinochilius	Winter sea ice	Armand et al. (2005)
Chaetoceros	Stratified water and low salinity	Crosta et al. (1997), Armand et al. (2005)
resting spore	High-productivity environment	Leventer (1991)
Eucampia antarctica	Cold water, high Fe content, melting water from iceberg/glaciers	Burckle (1984), Allen (2014), Minzoni et al. (2015), Barbara et al. (2016), Thomas et al. (2019)
Fragilariopsis curta	Winter sea ice	Gersonde and Zielinski (2000), Crosta et al. (2008), Armand et al. (2005), Esper and Gersonde (2014)
Fragilariopsis	Cold open-water conditions	Cunningham et al. (1999)
obliquecostata	Winter and summer sea ice indicator	Gersonde and Zielinski (2000)
Fragilariopsis kerguelensis	Open ocean, good indicator of the influence of oceanic water	Crosta et al. (2005), Pike et al. (2008), Rigual-Hernández et al. (2015)
Thalassiosira antarctica	Cold water related to ice edge or short sea ice cover, near ice edge	Cunningham et al. (1999), Taylor et al. (2001), Buffen et al. (2007), Pike et al. (2009), Barbara et al. (2016), Borchers et al. (2016), Campagne et al. (2016)
Thalassiosira lentiginosa	Permanent open-ocean conditions, indicator of warm water intrusion	Crosta et al. (2005), Rigual-Hernández et al. (2015), Campagne et al. (2016)
Thalassiosira oliverana	Permanent open-ocean conditions, indicator of warm water intrusion	Crosta et al. (2005), Rigual-Hernández et al. (2015), Campagne et al. (2016)
Paralia sulcata	Extant thycolopelagic coastal diatom	Sjunneskog and Scherer (2005)
Foraminifera species		
N. pachyderma adult	Able to live in polar oceans, surviving in brine channels within sea ice under hyper-saline and low-temperature conditions	Spindler and Dieckmann (1986), Dieckmann et al. (1991), Bergami et al. (2008, 2009), Hendry et al. (2009), Mikis et al. (2019)
	Spring and summer Antarctic conditions	
N. pachyderma juveniles	Winter Antarctic conditions	Mikis et al. (2019)
Alabaminella weddellensis	Upper slope–bathyal Southern Ocean	Mackensen et al. (1990, 1993)
	Phytodetritus feeder	Mackensen et al. (1994), Ishman and Szymcek (2003), Jorissen et al. (2007)
Epistominella	Upper slope–bathyal Southern Ocean	Mackensen et al. (1990, 1993)
exigua	CWD influence	Majewski et al. (2016, 2020)
	Opportunistic species (*r* strategist)	Gooday (1993), Thomas et al. (1995), Schmiedl et al. (1997), Wollenburg and Mackensen (1998)
	Phytodetritus feeder	Mackensen et al. (1994), Ishman and Szymcek (2003), Jorissen et al. (2007)
	Resistant to dissolution	Ishman and Szymcek (2003), Majewski et al. (2016, 2020)

Table 2. Continued.

	Ecology	References
Foraminifera species		
Cibicides spp., *Globocassidulina biora*, *G. subglobosa*, *Nonionella* spp., *Trifarina earlandi*	Sub-ice-shelf facies, from proximal to distal	Bart et al. (2016), McGlannan et al. (2017), Majewski et al. (2018), Prothro et al. (2018), Smith et al. (2019)
Miliammina earlandi	Agglutinated foraminifer dominate in open marine facies	Melis and Salvi (2009), Majewski et al. (2018, 2020)
T. earlandi	High hydrodinamism	Mackensen et al. (1990), Violanti (1996)
	Ice edge environment	Ishman and Szymcek (2003)
Silicoflagellate species		
S. speculum var. *monospicata*, var. *bispicata* and var. *speculum*	Open-water indicators	Malinverno (2010)
S. speculum var. *coronata*	Sea-ice-related	Malinverno et al. (2016)

imens per gram each at 18.3 ka; Fig. 4). *Neogloboquadrina pachyderma* is the only calcareous planktic foraminifera able to live in polar oceans, surviving in brine channels within sea ice under hyper-saline and low-temperature conditions (Table 2). In the autumn, when few adults reach gametogenesis, the juveniles living in the upper part of the water column become incorporated into the forming frazil ice (Spindler and Dieckmann, 1986). These juveniles can survive within sea ice cavities and brine channels (Dieckmann et al., 1991) since the sea ice can play the role of "nursery" or refuge from many predators (Lipps and Krebbs, 1974; Dieckmann et al., 1991). During the spring ice melting, individuals (adults and juveniles) are released into the water column and continue their life cycle (Dieckmann et al., 1991); the juveniles can grow in size and reach the reproductive maturity. The study on the ecology of *N. pachyderma* at the western Antarctic Peninsula recently documented by Mikis et al. (2019) evidenced that encrusted specimens reflect spring and summer conditions, while smaller non-encrusted specimens document autumn and winter conditions. Consequently, the contemporaneous occurrence of different test sizes and morphology in the studied sediments likely reflects the accumulation of different seasons. Thus, we interpret their occurrence to be the result of environmental conditions characterized by the beginning of open water with seasonal sea ice conditions.

In the time interval 20.8–18.1 ka, the sand content decrease suggests an environment evolving toward lower glacial influence than the previous time interval. The increasingly distal glacial influence probably favored calcareous-rich deposits, as also indicated by the increasing sedimentation rate reaching a mean value of 0.14 mm yr^{-1} for the period 20.3–18.1 ka (Table 1).

Similar results of a continuous deposition of planktic foraminifera-bearing, IRD-rich sediment layers were reported by Bonaccorsi et al. (2007) and Kim et al. (2020) on the continental slope of the Ross Sea east of the Iselin Bank from 28.2 to 17.2 ka (as uncorrected ages) and the western flank of the Iselin Bank at around 20 ka, respectively. Bonaccorsi et al. (2007) argued that these layers were deposited during a massive destabilization of the Ross ice shelf–sea ice system, likely caused by the meltwater pulse (MWP) at 19 ka. An alternative hypothesis was provided by Smith et al. (2010), who explained the significant occurrence of benthic and planktic foraminifera during glacial conditions (i.e., late MIS 3 and MIS 2, including the LGM) related to the presence of several polynyas along the Antarctic continental slope of both the Weddell and Ross Sea. Kim et al. (2020) suggested that the planktic foraminifera occurred mostly during the glacial periods and that they were deposited under cold and extensive sea ice conditions in close proximity to ice shelves or grounded ice sheet margins providing meltwater.

According to several authors (Anderson et al., 2002; Livingstone et al., 2012; Bentley et al., 2014; Yokoyama et al., 2018), the deglaciation after the LGM in the Antarctic region did not start at the same time, even if an atmospheric warming starting at around 18 ka was recorded at the Epica Dome C site (Jouzel et al., 2001). However, the timing and pattern of post-LGM ice sheet retreat in Antarctica are ambiguous and in many areas not well-constrained. As for the western Ross Sea, the Drygalski Basin paleo-ice stream reached its maximum position just north of Coulman Island on the middle to outer shelf, and it is thought to have receded by $\sim$ 14.0 cal ka BP (Frignani et al., 1998; Domack et al., 1999; Brambati et al., 2002). The JOIDES Basin paleo-ice stream

reached its maximum extent on the middle to outer shelf during the LGM (Licht et al., 1996; Domack et al., 1999; Shipp et al., 1999, 2002) and experienced open marine conditions by 13.0 cal ka BP (Domack et al., 1999; Melis and Salvi, 2009; Prothro et al., 2020). For the Central Basin east of the Hallett Ridge, Tolotti et al. (2013) indicated that the first deglaciation phased after the LGM in a period older than 19.3 ka (uncalibrated). If in the Hallett Ridge region, the first evidence of the deglaciation after the LGM started from approximately 20.3 ka, this is consistent with the time-transgressive character of the ice shelf retreat from north to south, as already evidenced by Anderson et al. (2014) and Halberstadt et al. (2016).

The stable oxygen isotope composition of *N. pachyderma* reveals a shift toward higher values between 19.1 and 18.1 ka (from 5.00 ‰ to 5.26 ‰; Fig. 4) in comparison with the previous period (20.5–19.2 ka) in which the values are on average below 5.00 ‰. This result is consistent with a cooling trend in surface-water masses. Superimposed on this general trend, there is evidence of smaller-amplitude δ^{18}O fluctuations of up to 0.3 ‰. The δ^{18}O signal of water masses in proximity to the Antarctic ice shelves is not only a function of temperature but is also strongly affected by salinity. In general, the δ^{18}O of surface waters is linearly related to surface salinity, since the same processes within the hydrological cycle responsible for salinity differences between water masses also result in δ^{18}O differences; these processes are mainly the ratio of evaporation and precipitation acting on surface-water masses and the amount of meteoric water stored in continental ice caps (Craig and Gordon, 1965). Meteoric and glacial meltwater supply along the coast, as a result of the glacial discharge and ice shelf deglaciation, may have contributed to the low planktic δ^{18}O excursions recorded during this time at our core location. In particular, the lightening of δ^{18}O to the value of 5.00 ‰ at 18.7 ka could record the meltwater influence related to the 19 ± 0.25 ka MWP event also reported in the Antarctic Peninsula (20–19 ka) by Heroy and Anderson (2007) and Xiao et al. (2016). Considering that the analyzed specimens (with a thick calcite crust) have been observed to be more abundant in the austral spring and summer than in winter (Mikis et al., 2019), we infer that our isotopic results reflect the warmest time of the year and the complete disappearance or reduction of sea ice when environmental conditions were optimal for growth and reproduction.

Together with the high content of planktic species, we also observe a significant increase in benthic foraminifera from 19.9 to 18.1 ka. They are mainly represented by *Cibicides* spp., *Globocassidulina biora* (type 4, small forms with a single aperture; sensu Majewski and Pawlowski, 2010), *G. subglobosa*, *Nonionella* spp., and *T. earlandi* species, which are commonly considered diagnostic of sub-ice-shelf facies (from proximal to distal) (Table 2). In this period, an occurrence of more than 20 % *E. exigua* and *A. weddellensis* is also evidenced. These two small taxa generally occur in the deep Atlantic and upper slope–bathyal Southern Ocean under the influence of the AABW (Table 2). Furthermore, they are considered opportunistic species (*r* strategist) able to feed on fresh phytodetritus (Table 2) that are adapted to food-limited areas where sea ice hinders the seasonal accumulation of phytodetritus (Table 2). The benthic foraminifera association seems to indicate conditions of distal sub-ice-shelf environments, although the occurrence of *E. exigua*, together with *A. weddellensis*, suggests the possible conditions near the southern limit of open marine environments, in agreement with Majewski et al. (2020). Another possibility is that these small species may indicate the occasional occurrence of CDW. In particular, it is thought that *E. exigua* may be related to these warmer waters, as suggested by Majewski et al. (2016, 2020).

During the same investigated time interval (20.8 ka to 18.1 ka), ADA continues to be low, and the diatom assemblage is very similar to the previous period. However, in this period there is a greater presence of *F. curta*, *F. obliquecostata*, *T. antarctica*, and *A. actinocyclus*, while *E. antarctica* var. *recta* is very abundant, especially at the end of the considered period (Fig. 5). *F. curta*, *F. obliquecostata*, and *A. actinochilus* are commonly reported as sea-ice-related species (Table 2). More in detail, *F. curta* is used as a proxy for winter sea ice; meanwhile, the high abundance of *F. obliquecostata* is used as a proxy for both winter and summer sea ice (Table 2). On the other hand, Cunningham et al. (1999) studied a diatom assemblage from the western Ross Sea and suggested that *F. obliquecostata* is also related to cold open water. *T. antarctica* is associated with cold water related to an ice edge or short sea ice cover (Table 2). *E. antarctica* var. *recta* thrives in nutrient-rich water, particularly with high Fe content, near the sea ice or in proximity to ice melting (Table 2). CRS content suggests limited sea ice extensions and/or shorter durations for this period (Table 2). *Chaetoceros hyalochaete* thrives under the environmental influence of highly stratified water due to melting water from ice and the enrichment of nutrients, typically during the austral spring bloom (Maddison et al., 2005), and forms resting spores (CRS) in response to unfavorable conditions (e.g., nutrient depletion). However, in the marine sediment sequences high values of CRS are related to stratified water and nutrient presence (Table 2).

To conclude, the co-presence of *T. antarctica* and *F. obliquecostata* (cold water indicators), together with the sea ice indicators *F. curta* and *A. actinochilus* and the abundance of CRS (Fig. 5), still suggests proximity to the calving zone, with a high iceberg presence (high IRD content) and the development of seasonal sea ice conditions (Fig. 6).

5.2 Deglacial period (time interval 18.1–11.6 ka)

A significant decrease in foraminifera concentration, both planktic and benthic, occurs at 17.9 ka, when an abrupt increase in diatom content and the first occurrence of silicoflagellates are observed at around 18 ka (Figs. 4, 5). The cold and

sea ice diatoms are abruptly replaced by open-water forms, such as *F. kerguelensis* (Table 2), reaching approximately 34 % abundance at 17.7 ka (Fig. 5). The sudden increase in CRS observed in this interval indicates increased nutrient input to the surface water (Table 2).

Silicoflagellate assemblages of *S. speculum* are dominated by permanently open-water varieties (*S. speculum* var. *monospicata*, var. *bispicata*, and var. *speculum*; Table 2), with a low contribution of sea-ice-related ones (*S. speculum* var. *coronata*; Table 2) that are only significant from 18.1 to 17.8 ka (Fig. 5). Overall, the floral change evidenced at 17.8 ka suggests prolonged open-ocean conditions, in agreement with Crosta et al. (2005) and Mezgec et al. (2017), and/or a strong intrusion of relatively warm and nutrient-rich oceanic water (Fig. 6). Additionally, the contemporaneous decrease in *E. antarctica* and *T. antarctica* supports the reduced presence of sea ice and the increased distance of the calving zone. Ameliorated climate conditions are also well-documented by an abrupt decrease in *N. pachyderma* δ^{18}O values (minimum value of 4.7 ‰ at 17.8 ka) (Fig. 4). We correlate this event with the first step of deglaciation, Termination 1a, as also reported in the Atlantic and Indian sectors of the Southern Ocean (Xiao et al., 2016). It is worthy of note that the warming in the Hallett Ridge area is more rapid with respect to the other areas: a maximum abundance of silicoflagellate open-ocean species is reached at 17.7 ka (Fig. 5) and remains high throughout the subsequent interval, coinciding with the Antarctic Isotope Maximum (AIM) 1 (Xiao et al., 2016).

At around 17.7 ka, ADA reaches its maximum value (242.0×10^6 v gdw^{-1}) and a moderate increase in ASA (0.7×10^6 s gdw^{-1}) is recorded. Although ADA values are slightly lower than those normally recorded in the Southern Ocean in the northwestern Ross Sea (e.g., Esper et al., 2010; Nair et al., 2015; Barbara et al., 2016), the values recorded in our sample are in agreement with other cores collected in this area (Tolotti et al., 2013; Maas, 2012; Mezgec, 2015; Kim et al., 2020).

The increase in biosilica values, probably related to the increase in primary productivity in surface waters compared to the previous period, is accompanied by the maximum abundance of phytodetritus benthic foraminifera (*E. exigua* and *A. weddellensis*) persisting up to 15.1 ka (Fig. 4), suggesting a more continuous influence of the CDW (Table 2). The increase in primary productivity is also supported by the sediment TOC content, which at this time reaches the maximum value of 0.5 %, confirming that the modest increase in productivity is mainly due to siliceous organisms (Figs. 4, 5). Additionally, the general decrease in benthic calcareous species and the relatively high percentages of *E. exigua* could indicate an increase in carbonate dissolution, since this species is known to be resistant to dissolution. Moreover, the high accumulation of organic matter at the seafloor could favor carbonate test corrosion, as evidenced in the literature (Kawahata et al., 2019), explaining the decreasing occurrence of carbonate foraminiferal shells at this time. High-productivity conditions, together with high organic carbon content in the sediments, could trigger carbonate dissolution for increasing dissolved CO_2.

The carbon isotope record of *N. pachyderma* shows a generally increasing trend from ∼ 19.1 ka toward a distinct maximum of 0.4 ‰ at around 17.8 ka (Fig. 4). Higher planktic foraminiferal δ^{13}C values may result from an increase in plankton productivity, as phytoplankton can deplete the shallowest surface waters of ^{12}C; this reconstruction is in agreement with the observed increased abundance of the phytodetritus benthic foraminifera *E. exigua* and *A. weddellensis* at this site. The δ^{13}C composition of surface-water masses in the Southern Ocean, however, is not simply a function of nutrient cycles and biological productivity because gas exchange with the atmosphere also plays a role in determining its distribution (Lynch-Stieglitz et al., 1995). Air–sea exchange of CO_2 leaves surface waters enriched in ^{13}C if there is sufficient time for isotopic equilibration to occur, but the presence of an ice shelf cover reduces the foraminiferal δ^{13}C values by restricting air–sea gas exchange; seasonal sea ice cover has a similar effect, preventing significant gas exchange. The ice shelf proximity inferred in our reconstruction to the Hallett Ridge region before 20.2 ka, together with the presence of seasonal sea ice, may have contributed to the low *N. pachyderma* δ^{13}C values recorded during that time, and in this view, the following generally increasing trend of δ^{13}C would have at least partially resulted from the ice shelf farther away and the following intensified air–sea gas exchange. Dissolution on the ocean floor exerts an additional control on the isotopic composition of planktic foraminifera, as it first removes the lightweight thin-shelled individuals of a species population, which are also isotopically lighter, leaving the isotopic composition of the surviving population heavier (Erez, 1978). Removal of isotopically light calcite caused by increased dissolution, as inferred from the occurrence of *E. exigua*, can be ruled out as the reason for the *N. pachyderma* δ^{13}C shift toward its maximum value of 0.4 ‰ at around 17.8 ka because this would have resulted in higher *N. pachyderma* δ^{18}O values, but this is opposite to what is observed.

Following the *N. pachyderma* δ^{13}C maximum of 0.4 ‰ identified at around 17.8 ka, the carbon isotope signal shows a decreasing trend up to 15.6 ka (Fig. 4). This is the time interval when we inferred a more continuous influence of the CDW at our site location based on the high abundance of the benthic foraminifera *E. exigua* and *A. weddellensis* between 17.7 and 15.1 ka (Fig. 4). Foraminiferal δ^{13}C records are influenced, among other factors, by water-mass circulation, and the observed trend towards lower δ^{13}C values would be consistent with the intrusion of modified upper CDW upwelled into the shelf. However, considering the lower resolution of our isotope record in this part of the sedimentary sequence and without a parallel reconstruction of the benthic foraminifera δ^{13}C ratios confirming the carbon isotope signa-

ture of the CDW at our site location, the explanation for the *N. pachyderma* δ^{13}C depletion involving a direct response to changing water-mass circulation remains speculative.

After the sudden increase in abundance at around 17.5 ka, siliceous microorganisms decrease again. Thus, the gradual decrease in *F. kerguelensis* and CRS, corresponding to an increase in *E. antarctica* var. *recta*, together with a slight increase in *A. actinochilus* and *F. curta* at around 13.8 ka, could represent the cooling associated with the Antarctic Cold Reversal (ACR) (Fig. 6). This cooling and sea ice increase, however, are of short duration and are not recorded by the silicoflagellate assemblages.

Despite the foraminifera decline, a significant occurrence of *T. earlandi* is recorded from 18.0 to approximately 11.3 ka. In the Antarctic environment, this foraminifer represents conditions of the sub-ice-shelf when associated with other species such as *Globocassidulina* spp. and *Cibicides* spp. (Table 2), but its dominance is related to the ice edge environment in the Larsen Ice Shelf of the Antarctic Peninsula (Ishman and Szymcek, 2003) and to the ice shelf retreat in the southern cores of the JOIDES Basin (Melis and Salvi, 2009; Majewski et al., 2020). Nevertheless, in the outer shelves and upper slope areas, this taxon has been reported as being typical of sandy substrates reflecting relatively high bottom-water current velocities (Table 2). The rare presence of IRD testifies to the occasional presence of icebergs far from the calving zone.

In our case, the presence of slight millimeter laminations occurring in the sediments of this period and running out at around 7.5 ka suggests the onset of weak bottom currents, promoting the dominance of *T. earlandi* at least until 10.2 ka. The onset of the major influence of a bottom current is also supported by a slight improvement in the total sediment sorting (Fig. 3), suggesting the presence of currents that, although weak, are able to select the sediment. The decrease in sand content in the laminated layers is probably related to the lower input of IRD. In the sediment younger than 7.5 ka, the laminations tend to disappear, and the bottom currents are not strong enough to sort out the coarse sediment arriving there.

5.3 Time interval 11.6–2.0 ka, interglacial

Lithological changes and calcareous microfauna document the establishment of different conditions by 11.6 ka. Planktic foraminifera strongly decrease and disappear almost completely from 10.2 ka, while benthic foraminifera, though considerably diminished, are still represented by a significant presence of *E. exigua* and *T. earlandi* (Fig. 4). The diatom assemblage is characterized from 11.6 to 7.5 ka by a slight decrease in the open-water species *F. kerguelensis* and by the persistence of low diatom abundance (Fig. 5), suggesting environmental conditions not favorable for diatom growth. With the exception of a short-lived increase in sea-ice-related silicoflagellate varieties at 10.2 ka, silicoflagellate assemblages are dominated by open-ocean varieties (*S. speculum* var. *speculum*, var. *monospicata*, var. *bispicata* $> 50\,\%$) throughout this interval (Fig. 5) that correspond to the timing of the second step of deglaciation, Termination 1b, leading to the Antarctic early Holocene Optimum, as recorded in the Atlantic and Indian sectors of the Southern Ocean by the maxima of diatom warm water species (Xiao et al., 2016). In our record, however, the signal of diatom warm water species is masked by the increase in CRS, which, together with the high value of TOC and the low ratio of C / N, supports open-ocean conditions with stratified waters that may linked to sea ice melting (Figs. 3 and 5; Table 2). This interval coincides with the warm early Holocene period, evidenced by Etourneau et al. (2013) in the Antarctic Peninsula, which is characterized by warm upper-ocean temperatures with reduced seasonal sea ice (Alley et al., 2010; Pike et al., 2013).

Calcareous foraminifera, both planktic and benthic, become nearly absent or rare during the Holocene, when temperatures were significantly warmer and sea ice was reduced compared to the last glacial period, as suggested by the increasing occurrence of the relatively warm water species *F. kerguelensis*. At our site, we speculate that these features are the result of a calving zone farther away and the presence of an efficient contour current corresponding to the Early Holocene Temperature Maximum (11.6–8.5 ka – Masson et al., 2000; Mezgec et al., 2017). The increasing sand and IRD contents by 7.5 ka still suggest the increasing transit of icebergs in this zone. The dominance of agglutinated benthic foraminifera, mainly represented by *Miliammina earlandi*, suggests that dissolution, rather than a lack of production or dilution, was the main controlling factor on calcareous test accumulation and preservation. Holocene dissolution may have been driven by a lower carbonate ion concentration in the deep water, presumably the HSSW, or within sediment pore water related to high fluxes of organic carbon from surface-water productivity (e.g., Wollenburg and Kuhnt, 2000; Capotondi et al., 2020). During the interglacial, the Antarctic sediments lack carbonates (Grobe and Mackensen, 1992) although productivity is enhanced. The high flux of organic matter produced during the interglacial periods, in fact, increases the CO_2 content in the water masses, presumably the HSSW, flowing downslope and in the interstitial waters, enhancing the solution of carbonate (Kawahata et al., 2019). The disappearance of the calcareous foraminifera and the dominance of *M. earlandi*, agglutinated in open marine facies, have been documented in the diatomaceous sediments of the Ross Sea troughs by Salvi et al. (2004), Melis and Salvi (2009), and Majewski et al. (2018, 2020) (as *M. arenacea*) during the Late Pleistocene–Holocene transition. This "regional" event is not synchronous, since in the western Ross Sea it was recorded in the southern JOIDES Basin (core ANTA96-8; Melis and Salvi, 2009), where the barren level is located between 13.5 and 21.0 ka (not calibrated ages). Afterward, the disappear-

ance of calcareous foraminifera is documented from 12.3 and 10.5 ka (not calibrated ages) in the northern JOIDES Basin (ANTA91-14 and ANTA99-J5 cores, respectively) and finally in the ANTA96-9 core, located in the southern JOIDES Basin, at 6.3 ka (Melis and Salvi, 2009).

Between 7.5 and 3.5 ka, the siliceous assemblages show an increase in ADA, a peak in ASA, and fluctuating abundances of sea-ice-related species among both diatoms and silicoflagellates, testifying to highly varying sea ice conditions. Although in other records from the Southern Ocean a cooling trend is observed in this period (Hodell et al., 2001; Shewenell et al., 2011; Xiao et al., 2016), the relatively high abundance of *F. kerguelensis* does not suggest a significant cooling in this interval. From 3.5 ka, the decrease in the abundance of silicoflagellates and, among diatoms, *F. kerguelensis* and CRS suggests an environmental change (Fig. 5). In fact, at the same time, the increase in *F. curta* and ice-related silicoflagellates suggests the beginning of the Neoglacial period, which starts at around 4 ka, in agreement with Xiao et al. (2016), Mezgec et al. (2017), and references therein. In this interval, the increase in sand content testifies to a strengthening of the bottom current also supported by the increase in the abundance of the coastal fossil diatom *P. sulcata* (Fig. 6). This is a tycopelagic coastal species considered extinct in Antarctica (Table 2). Its occurrence in this interval likely indicates that it was transported from the coastal area to the continental margin during glacial expansion and accumulated there as reworked by the currents. In addition, the increase in IRD suggests more glacial transport by icebergs.

6 Conclusions

Integrated micropaleontological (planktic and benthic foraminifera, diatoms, and silicoflagellates) analysis together with textural and geochemical results of a deep-sea core from the Hallett Ridge (northwestern Ross Sea) provide new data for the late Quaternary (23–2 ka) paleoenvironmental and paleoceanographic reconstructions of this region. We investigate a sedimentary interval characterized by the presence of rich and well-preserved calcareous foraminiferal assemblages corresponding to the last glacial–Holocene. The age model was performed by combining AIOM and carbonate radiocarbon dating. In particular, the availability of well-preserved calcareous planktic foraminiferal content from 18 to 15 ka allowed us to make advances in reconstructing an accurate age constraint of environmental changes during the early deglacial interval. In detail, several significant paleoenvironmental and paleoclimate changes were identified. From 22.6 to 20.8 ka the studied area was influenced by strong glacial conditions, likely related to the proximity of an ice shelf and the beginning of the deglaciation. A massive input of terrigenous sediments, including IRD, which largely diluted the biogenic fraction in the sedimentary record determining environmental conditions hostile to bio-productivity and test preservation, characterized this period. A sharp recovery of productivity (mainly planktic and benthic foraminifera and diatoms) was evidenced at around 20.2 ka, when the co-occurrence of large *N. pachyderma* tests and juvenile forms in the deglacial sediments reflects more open-water conditions and/or variation in the duration and coverage of seasonal sea ice. The co-occurrence of sea ice indicators (e.g., *A. actinochilus*, *F. curta*) together with cold water indicators (e.g., *E. antarctica* var. *recta*, *T. antarctica*) supports the environmental interpretation. The lowest $\delta^{18}O$ value at 18.7 ka suggests a glacial meltwater supply likely related to the 19 ± 0.25 ka MWP event.

At around 18 ka the cold and sea ice diatoms are abruptly replaced by warm water species. An optimum of the surface-water temperature together with an increase in productivity also indicate a pronounced increase in the abundance of silicoflagellates, mainly represented by open-water species. The increasing productivity in the water column is also evidenced by the increasing carbon isotope signal of *N. pachyderma* and the abundance of phytodetritus benthic foraminifera. The diatom assemblage indicates cooling conditions at around 13.8 ka correlatable with the Antarctic Cold Reversal, while on the seafloor, the benthic foraminifera *T. earlandi* marks the occurrence of contour currents that characterized this period, which lasts until around 7.5 ka. During the Holocene the calcareous foraminiferal content experienced a dramatic decrease, suggesting the presence of dissolution conditions. The Neoglacial cold climatic phase was characterized by an increase in sea-ice-related diatoms and silicoflagellates at about 4.0 ka and by an increase in sand content, suggesting a strengthening of the bottom current, also supported by the increase in the abundance of the fossil diatom *P. sulcata*, which was transported from coastal regions.

This study highlights the fact that the integrated use of diverse microfossil proxies is important to reconstruct the main paleoenvironmental and paleoclimate variations of polar areas. Furthermore, our data confirm that the availability of well-preserved calcareous material represents an excellent opportunity to construct a reliable age model for the deglacial period.

Data availability. All data pertinent to this paper are given within the paper and in Tables S1 and S2.

Supplement. The supplement related to this article is available online at: https://doi.org/10.5194/jm-40-15-2021-supplement.

Author contributions. EC, LC, and RM were responsible for conceptualization, methodology, investigation, writing the original draft, and review and editing. Micropaleontological analyses are by LC, RM, AG (foraminifera), FT (diatoms), and EM (silicoflagel-

lates), with stable isotopes by PF. Sedimentological analyses are by EC and TOC, with $CaCO_3$ analyses by BKK. JKH and SK contributed to the geophysical data interpretation. EC and BKK acted as project leaders and acquired funding. All authors contributed to the interpretation of the results and the writing of the original draft.

Competing interests. The authors declare that they have no conflict of interest.

Acknowledgements. We sincerely thank the technicians, captain, and crew of IBRV *Araon* for their efforts in obtaining sediment samples and geophysical data during the ANA03B expedition. We would like to thank the PNRA (Progetto Nazionale di Ricerca in Antartide) and KOPRI (Korean Polar Research Institute) for funding the campaign. The authors would like to thank Karin Mezgec for the first set of diatom analyses. This research used samples provided by the Sorting Center–Trieste Section of the Museo Nazionale dell'Antartide, and it is developed in the framework of the STREAM project (Late Quaternary evolution of the ocean–ice sheet interactions: the record from the Ross Sea continental margin, Antarctica). Ester Colizza and Boo-Keun Khim wish to express their appreciation to the Italian Ministry of Foreign Affairs and International Cooperation (MAECI PGR 00822 and 01060) for the PNRA project (2010/A2.07) and the National Research Foundation of Korea (2019K1A3A1A25000116) for the KOPRI project (PE21090). Many thanks to Karolyn Close for the linguistic revision of an earlier version of the paper. We sincerely thank the editor, the anonymous reviewer, and Wojciech Majewski for their useful comments, which improved the paper.

Financial support. This work has been designed in the framework of the STREAM project. This project is co-funded by a grant from the Italian Ministry of Foreign Affairs and International Cooperation and the National Research Foundation of Korea (Korea–Italy Joint Research Program). This research is contribution no. 2038 of CNR-ISMAR.

Review statement. This paper was edited by Sev Kender and reviewed by Wojciech Majewski and one anonymous referee.

References

Allen, C. S.: Proxy development: a new facet of morphological diversity in the marine diatom Eucampia antarctica (Castracane) Mangin, J. Micropalaeontol., 33, 131–142, https://doi.org/10.1144/jmpaleo2013-025, 2014.

Alley, R. B., Andrews, J. T., Brigham-Grette, J., Clarke, G. K. C., Cuffey, K. M., Fitzpatrick, J. J., Funder, S., Marshall, S. J., Miller, G. H., Mitrovica, J. X., Muhs, D. R., Otto-Bliesner, B. L., Polyak, L., and White, J. W. C.: History of the Greenland Ice Sheet: Paleoclimatic insights, Quaternary Sci. Rev., 29, 1728–1756, https://doi.org/10.1016/j.quascirev.2010.02.007, 2010.

Anderson, J. B., Shipp, S. S., Lowe, A. L., Wellner, J. S., and Mosola, A. B.: The Antarctic ice sheet during the last Glacial Maximum and its subsequent retreat history: a review, Quaternary Sci. Rev., 21, 49–70, https://doi.org/10.1016/S0277-3791(01)00083-X, 2002.

Anderson, J. B., Conway, H., Bart, P. J., Witus, A. E., Greenwood, S. L., McKay, R. M., Hall, B. L., Ackert, R. P., Licht, K., Jakobsson, M., and Stone, J. O.: Ross sea paleo-ice sheet drainage and deglacial history during and since the LGM, Quaternary Sci. Rev., 100, 31–54, 2014.

Anderson, J. B., Simkins, L. M., Bart, P. J., De Santis, L., Halberstadt, A. R. W., Olivo, E., and Greenwood, S. L.: Seismic and geomorphic records of Antarctic Ice Sheet evolution in the Ross Sea and controlling factors in its behaviour, in: Glaciated Margins: The Sedimentary and Geophysical Archive, edited by: Le Heron, D. P., Hogan, K. A., Phillips, E. R., Huuse, M., Busfield, M. E., and Graham, A. G. C., Geological Society of London Special Publication, London, UK, https://doi.org/10.1144/SP475.5, 2018.

Andrews, J. T., Domack, E. W., Cunningham, W. L., Leventer, A., Licht, K. J., Jull, A. J. T., DeMaster, D. J., and Jennings, A. E.: Problems and possible solutions concerning radiocarbon dating of surface marine sediments, Ross Sea, Antarct. Quat. Res., 52, 206–216, https://doi.org/10.1006/qres.1999.2047, 1999.

Armand, L. K.: The use of diatom transfer functions in estimating sea-surface temperature and sea-ice in cores from the southeast Indian Ocean, PhD thesis, Australian National University, Canberra, Australia, 537 pp., 1997.

Armand, L. K., Crosta, X., Romero, O., and Pichon, J.-J.: The biogeography of major diatom taxa in Southern Ocean sediments. 1. Ice-related species, Palaeogeogr. Palaeocl., 223, 93–126, https://doi.org/10.1016/j.palaeo.2005.02.015, 2005.

Arndt, J. E., Schenke, H. W., Jakobsson, M., Nitsche, F., Buys, G., Goleby, B., Rebesco, M., Bohoyo, F., Hong, J. K., Black, J., Greku, R., Udintsev, G., Barrios, F., Reynoso-Peralta, W., Morishita, T., and Wigley, R.: The International Bathymetric Chart of the Southern Ocean (IBCSO) Version 1.0 – A new bathymetric compilation covering circum-Antarctic waters, Geophys. Res. Lett., 40, 3111–3117, https://doi.org/10.1002/grl.50413, 2013.

Barbara, L., Crosta, X., Leventer, A., Schmidt, S., Etourneau, J., Domack, E., and Massé, G.: Environmental responses of the Northeast Antarctic Peninsula to the Holocene climate variability, Paleoceanography, 31, 131–147, https://doi.org/10.1002/2015PA002785, 2016.

Bart, P. J., Coquereau, L., Warny, S., and Majewski, W.: In situ foraminifera in grounding zone diamict: a working hypothesis, Antarct. Sci., 28, 313–321, https://doi.org/10.1017/S0954102016000055, 2016.

Bart, P. J., DeCesare, M., Rosenheim, B. E., Majewski, W., and McGlannan, A.: A centuries-long delay between a paleo-ice-shelf collapse and grounding-line retreat in the Whales Deep Basin, eastern Ross Sea, Antarctica, Sci. Rep., 8, 12392, https://doi.org/10.1038/s41598-018-29911-8, 2018.

Bentley, M. J., Cofaigh, C. Ó., Anderson, J. B., Conway, H., Davies, B., Graham, A. G. C., Hillebrand, C.-D., Hodgson, D. A., Jamieson, S. S. R., Larter, R. D., Mackintosh, A., Smith, J. A., Verleyen, E., Ackert, R. P., Bart, P. J., Berg, S., Brunstein, D., Canals, M., Colhoun, E. A., Crosta, X., Dickens, W. A., Domack, E., Dowdeswell, J. A., Dunbar, R., Ehrmann, W., Evans, J., Favier, V., Fink, D., Fogwill, C. J., Glasser, N. F., Gohl, K., Golledge, N. R., Goodwin, I., Gore, D. B., Greenwood, S. L.,

Hall, B. L., Hall, K., Hedding, D. W., Hein, A. S., Hocking, E. P., Jakobsson, M., Johnson, J. S., Jomelli, V., Jones, R. S., Klages, J. P., Kristoffersen, Y., Kuhn, G., Leventer, A., Licht, K., Lilly, K., Lindow, J., Livingstone, S. J., Massé, G., McGlone, M. S., McKay, R. M., Melles, M., Miura, H., Mulvaney, R., Nel, W., Nitsche, F. O., O'Brien, P. E., Post, A. L., Roberts, S. J., Saunders, K. M., Selkirk, P. M., Simms, A. R., Spiegel, C., Stolldorf, T. D., Sugden, D. E., van der Putten, N., van Ommen, T., Verfaillie, D., Vyverman, W., Wagner, B., White, D. A., Witus, A. E., and Zwartz, D., the RAISED consortium: A community-based geological reconstruction of Antarctic Ice Sheet deglaciation since the Last Glacial Maximum, Quaternary Sci. Rev., 100, 1–9, https://doi.org/10.1016/j.quascirev.2014.06.025, 2014.

Bergami, C., Capotondi, L., Sprovieri, M., Tiepolo, M., Langone, L., Giglio, F., and Ravaioli, M.: Mg / Ca ratios in the planktonic foraminifer *Neogloboquadrina pachyderma* (sinistral) from plankton tows in the Ross Sea and the Pacific sector of the Southern Ocean (Antarctica): comparison of different methodological approaches, Chem. Ecol., 24, 39–46, https://doi.org/10.1080/02757540801963303, 2008.

Bergami, C., Capotondi, L., Langone, L., Giglio, F., and Ravaioli, M.: Distribution of living planktonic foraminifera in the Ross Sea and the Pacific sector of the Southern Ocean (Antarctica), Mar. Micropaleontol., 73, 37–48, https://doi.org/10.1016/j.marmicro.2009.06.007, 2009.

Blaauw, M.: Methods and code for "classical" age-modelling of radiocarbon sequences, Quat. Geochronol., 5, 512–518, https://doi.org/10.1016/j.quageo.2010.01.002, 2010.

Bonaccorsi, R., Quaia, T., Burckle, L. H., Anderson, R. F., Melis, R., and Brambati, A.: C-14 age control of pre- and post-LGM events using *N. pachyderma* preserved in deep-sea sediments (Ross Sea, Antarctica), in: Proceedings of the 10th ISAES X, USGS, Santa Barbara, USA, 26 September–1 October 2007, 2007–1047, https://doi.org/10.3133/of2007-1047, 2007.

Borchers, A., Dietze, E., Kuhn, G., Esper, O., Voigt, I., Hartmann, K., and Diekmann, B.: Holocene ice dynamics and bottom-water formation associated with Cape Darnley polynya activity recorded in Burton Basin, East Antarctica, Mar. Geophys. Res., 37, 49–70, https://doi.org/10.1007/s11001-015-9254-z, 2016

Brambati, A., Melis, R., Quaia, T., and Salvi, G.: Late Quaternary climatic changes in the Ross Sea area, Antarctica, in: Proceedings of the 8th International Symposium on Antarctic Earth Sciences, Wellington, New Zealand, 5–9 July 1999, 359–364, 2002.

Budillon, G., Castagno, P., Aliani, S., Spezie, G., and Padman, L.: Thermohaline variability and Antarctic bottom water formation at the Ross Sea shelf break, Deep-Sea Res., 58, 1002–1018, https://doi.org/10.1016/j.dsr.2011.07.002, 2011

Buffen, A., Leventer, A., Rubin, A., and Hutchins, T.: Diatom assemblages in surface sediments of the northwestern Weddell Sea, Antarctic Peninsula, Mar. Micropaleontol., 62, 7–30, https://doi.org/10.1016/j.marmicro.2006.07.002, 2007.

Burckle, L. H.: Ecology and paleoecology of the marine diatom *Eucampia antarctica* (Castr.) Mangin, Mar. Micropaleontol., 9, 77–86, https://doi.org/10.1016/0377-8398(84)90024-0, 1984.

Campagne, P., Crosta, X., Schmidt, S., Noëlle Houssais, M., Ther, O., and Massé, G.: Sedimentary response to sea ice and atmospheric variability over the instrumental period off Adélie Land, East Antarctica, Biogeosciences, 13, 4205–4218, https://doi.org/10.5194/bg-13-4205-2016, 2016.

Capotondi, L., Bonomo, S., Budillon, G., Giordano, P., and Langone, L.: Living and dead benthic foraminiferal distribution in two areas of the Ross Sea (Antarctica), Rend. Lincei-Sci. Fis., 31, 1037–1053, https://doi.org/10.1007/s12210-020-00949-z, 2020.

Castagno, P., Capozzi, V., DiTullio, G. R., Falco, P., Fusco, G., Rintoul, S. R., Spezie, G., and Budillon, G.: Rebound of shelf water salinity in the Ross Sea, Nat. Commun., 10, 5441, https://doi.org/10.1038/s41467-019-13083-8, 2019.

Clark, P. U., Dyke, A. S., Shakun, J. D., Carlson, A. E., Clark, J., Wohlfarth, B., Mitrovica, J. X., Hostetler, S. W., and McCabe, A. M.: The Last Glacial Maximum, Science, 325, 710–714, https://doi.org/10.1126/science.1172873, 2009.

Colleoni, F., De Santis, L., Montoli, E., Olivo, E., Sorlien, C. C., Bart, P. J., Gasson, E. G. W., Bergamasco, A., Sauli, C., Wardell, N., and Prato, S.: Past continental shelf evolution increased Antarctic ice sheet sensitivity to climatic conditions, Sci. Rep.-UK, 8, 11323, https://doi.org/10.1038/s41598-018-29718-7, 2018.

Craig, H. and Gordon, L. I.: Deuterium and oxygen-18 variations in the ocean and the marine atmosphere, in: Stable Isotopes in Oceanographic Studies and Paleotemperatures, edited by: Tongiorgi E., Laboratorio di Geologia Nucleare, Pisa, Italy, 9–130, 1965.

Crosta, X. and Koç, N.: Chapter Eight Diatoms: from micropaleontology to isotope geochemistry, in: Development in Marine Geology, 1, Proxies in late Cenozoic palaeoceanography, edited by: Hillaire-Marcel, C. and De Vernal, A., Elsevier, Amsterdam, The Nederlands, 327–369, https://doi.org/10.1016/S1572-5480(07)01013-5, 2007.

Crosta, X., Pichon, J.-J., and Labracherie, M.: Distribution of Chaetoceros resting spores in modern peri-Antarctic sediments, Mar. Micropaleontol., 29, 283–299, https://doi.org/10.1016/S0377-8398(96)00033-3, 1997.

Crosta, X., Romero, O., Armand, L. K., and Pichon, J. J.: The biogeography of the major diatom taxa in Southern Ocean sediments: 2. Open ocean related species, Palaeogeogr. Palaeocl., 223, 66–92, https://doi.org/10.1016/j.palaeo.2005.03.028, 2005.

Crosta, X., Denis, D., and Ther, O.: Sea ice seasonality during the Holocene, Adélie Land, East Antarctica, Mar. Micropaleontol., 66, 222–232, https://doi.org/10.1016/j.marmicro.2007.10.001, 2008.

Cunningham, W. L., Leventer, A., Andrews, J. T., Jennings, A. E., and Licht, K. J.: Late Pleistocene-Holocene marine conditions in the Ross Sea, Antarctica: evidence from the diatom record, Holocene, 9, 129–139, 1999.

DeJong, H. B., Dunbar, R. B., Mucciarone, D., and Koweek, D. A.: Carbonate saturation state of surface waters in the Ross Sea and Southern Ocean: controls and implications for the onset of aragonite undersaturation, Biogeosciences, 12, 6881–6896, https://doi.org/10.5194/bg-12-6881-2015, 2015.

Dieckmann, G. S., Spindler, M., Lange, M. A., Ackley, S. F., and Eicken, H.: Antarctic sea ice: a habitat for the foraminifer *Neogloboquadrina pachyderma*, J. Foram. Res., 21, 182–189, https://doi.org/10.2113/gsjfr.21.2.182, 1991.

Dinniman, M. S., Klinck, J. M., and Smith Jr., W. O.: A model study of Circumpolar Deep Water on the West Antarctic Peninsula and Ross Sea continental shelves, Deep-Sea Res., 58, 1508–1523, https://doi.org/10.1016/j.dsr2.2010.11.013, 2011.

Domack, E. W., Jacobson, E. A., Shipp, S., and Anderson, J. B.: Late Pleistocene-Holocene retreat of the West Antarctic Ice-Sheet system in the Ross Sea: Part 2 – sedimentologic and stratigraphic signature, Geol. Soc. Am. Bull., 111, 1517–1536, https://doi.org/10.1130/0016-7606(1999)111<1517:LPHROT>2.3.CO;2, 1999.

Erez, J.: The influence of differential production and dissolution on the stable isotope composition of planktonic foraminifera, PhD thesis, MIT-WHOI, Woods Hole, USA, 119 pp., 1978.

Esper, O. and Gersonde, R.: Quaternary surface water temperature estimations: New diatom transfer functions for the Southern Ocean, Palaeogeogr. Palaeocl., 414, 1–19, https://doi.org/10.1016/j.palaeo.2014.08.008, 2014.

Esper, O., Gersonde, R., and Kadagies, N.: Diatom distribution in southeastern Pacific surface sediments and their relationship to modern environmental variables, Palaeogeogr. Palaeocl., 287, 1–27, https://doi.org/10.1016/j.palaeo.2009.12.006, 2010.

Etourneau, J., Collins, L. G., Willmott, V., Kim, J.-H., Barbara, L., Leventer, A., Schouten, S., Sinninghe Damsté, J. S., Bianchini, A., Klein, V., Crosta, X., and Massé, G.: Holocene climate variations in the western Antarctic Peninsula: evidence for sea ice extent predominantly controlled by changes in insolation and ENSO variability, Clim. Past, 9, 1431–1446, https://doi.org/10.5194/cp-9-1431-2013, 2013.

Farmer, G. L., Licht, K., Swope, R. J., and Andrews, J. T.: Isotopic constraints on the provenance of fine-grained sediment in LGM tills from the Ross Embayment, Antarctica, Earth Planet. Sc. Lett., 249, 90–107, https://doi.org/10.1016/j.epsl.2006.06.044, 2006.

Folk, R. L. and Ward, W. C.: Brazos River bar: a study in the significance of grain size parameters, J. Sediment. Petrol., 27, 3–26, 1957.

Frank, T. D., James, N. P., Bone, Y., Malcolm, I., and Bobak, L. E.: Late Quaternary carbonate deposition at the bottom of the world, Sediment. Geol., 305, 1–16, https://doi.org/10.1016/j.sedgeo.2014.02.008, 2014.

Friedman, G. M. and Sanders, J. E.: Principles of Sedimentology, Wiley, New York, USA, 1978.

Frignani, M., Giglio, F., Langone, L., Ravaioli, M., and Mangini, A.: Late-Pleistocene – Holocene sedimentary fluxes of organic carbon and biogenic silica in the northwestern Ross Sea, Antarctica, Ann. Glaciol., 27, 697–703, https://doi.org/10.3189/1998AoG27-1-697-703, 1998.

Gersonde, R. and Zielinski, U.: The reconstruction of Late Quaternary Antarctic sea-ice distribution – the use of diatoms as a proxy for sea-ice, Palaeogeogr. Palaeocl., 162, 263–286, https://doi.org/10.1016/S0031-0182(00)00131-0, 2000.

Golledge, N. R., Menviel, L., Carter, L., Fogwill, C. J., England, M. H., Cortese, G., and Levy, R. H.: Antarctic contribution to meltwater pulse 1A from reduced Southern Ocean overturning, Nat. Commun., 5, 5107, https://doi.org/10.1038/ncomms6107, 2014.

Gooday, A. J.: Deep-sea benthic foraminiferal species which-exploit phytodetritus – characteristic features and controls on distribution, Mar. Micropaleontol., 22, 187–205, https://doi.org/10.1016/0377-8398(93)90043-W, 1993

Grobe, H. and Mackensen, A.: Late Quaternary climatic cycles as recorded in sediments from the Antarctic continental margin, in: The Antarctic Paleoenvironment: A Perspective on Global Change, edited by: Kennett, J. P. and Warkne, D. A., American Geophysical Union, Washington, D.C., United States, 349–376, 1992.

Halberstadt, A. R. W., Simkins, L. M., Greenwood, S. L., and Anderson, J. B.: Past ice-sheet behaviour: retreat scenarios and changing controls in the Ross Sea, Antarctica, The Cryosphere, 10, 1003–1020, https://doi.org/10.5194/tc-10-1003-2016, 2016.

Hall, B. L., Henderson, G. M., Baroni, C., and Kellogg, T. B.: Constant Holocene southern-ocean ^{14}C reservoir ages and ice-shelf flow rates, Earth Planet. Sc. Lett., 296, 115–123, https://doi.org/10.1016/j.epsl.2010.04.054, 2010.

Hauck, J., Gerdes, D., Hillenbrand, C.-D., Hoppema, M., Kuhn, G., Nehrke, G., Völker, C., and Wolf-Gladrow, D. A.: Distribution and mineralogy of carbonate sediments on Antarctic shelves, J. Marine Syst., 90, 77–87, https://doi.org/10.1016/j.jmarsys.2011.09.005, 2012.

Hendry, K. R., Rickaby, R. E., Meredith, M. P., and Elderfield, H.: Controls on stable isotope and trace metal uptake in *Neogloboquadrina pachyderma* (sinistral) from an Antarctic sea-ice environment, Earth Planet. Sci. Lett., 278, 67–77, https://doi.org/10.1016/j.epsl.2008.11.026, 2009.

Heroy, D. C. and Anderson, J. B.: Radiocarbon constraints on Antarctic Peninsula Ice Sheet retreat following the Last Glacial Maximum (LGM), Quaternary Sci. Rev., 26, 3286–3297, https://doi.org/10.1016/j.quascirev.2007.07.012, 2007.

Hillenbrand, C.-D., Smith, J. A., Kuhn, G., Esper, O., Gersonde, R., Larter, R. D., Maher, B., Moreton, S. G., Shimmield, T. M., and Korte, M.: Age assignment of a diatomaceous ooze deposited in the western Amundsen Sea Embayment after the Last Glacial Maximum, J. Quatern. Sci., 25, 280–295, https://doi.org/10.1002/jqs.1308, 2009.

Hodell, D. A., Kanfoush, S. L., Shemesh, A., Crosta, X., Charles, C. D., and Guilderson, T. P.: Abrupt cooling of Antarctic surface waters and sea ice expansion in the South Atlantic sector of the Southern Ocean at 5000 cal yr B.P., Quaternary Res., 56, 191–198, https://doi.org/10.1006/qres.2001.2252, 2001.

Igarashi, A., Numanami, H., Tsuchiya, Y., and Fukucki, M.: Bathymetric distribution of fossil foraminifera within marine sediment cores from the eastern part of Lutzow Holm Bay, East Antarctica, and its paleoceanographic implications, Mar. Micropaleontol., 42, 125–162, https://doi.org/10.1016/S0377-8398(01)00004-4, 2001.

Ishman, S. E. and Szymcek, P.: Foraminiferal distributions in the former Larsen-A Ice Shelf and Prince Gustav Channel region, eastern Antarctic Peninsula margin: a baseline for Holocene paleoenvironmental change, in: Antarctic Peninsula Climate Variability: Historical and Paleoenvironmental Perspectives, edited by: Domack, E., Levente, A., Burnet, A., Bindschadler, R., Convey, P., and Kirby, M., American Geophysical Union, Washington, D.C., United States, 239–260, https://doi.org/10.1029/AR079p0239, 2003.

Jacobs, S. S.: Marine controls on modern sedimentation on the Antarctic continental shelf, Mar. Geol., 85, 121–153, https://doi.org/10.1016/0025-3227(89)90151-5, 1989.

Jacobs, S. S.: Bottom water production and its links with the thermohaline circulation, Antarct. Sci., 16, 427–437, https://doi.org/10.1017/S095410200400224X, 2004.

Jordan, R. W. and McCartney, K.: *Stephanocha* nom. nov., a replacement name for the illegitimate silicoflagellate genus

Distephanus (Dictyochophyceae), Phytotaxa, 201, 177–187, https://doi.org/10.11646/phytotaxa.201.3.1, 2015.

Jorissen, F. J., Fontanier, C., and Thomas, E.: Paleoceanographical proxies based on deep-sea benthic foraminiferal assemblage characteristics, in: Proxies in Late Cenozoic, Paleoceanography, Developments in Marine Geology, edited by: Hillaire-Marcel, C. and De Vernal, A., Elsevier, Amsterdam, the Netherlands, 263–325, https://doi.org/10.1016/S1572-5480(07)01012-3, 2007.

Jouzel, J., Masson, V., Cattani, O., Falourd, S., Stievenard, M., Stenni, B., Longinelli, A., Johnsen, S. J., Steffenssen, J. P., Petit, J. R., Schwander, J., Souchez, R., and Barkov, N. I.: A new 27 ky high resolution East Antarctic climate record, Geophys. Res. Lett., 28, 3199–3202, https://doi.org/10.1029/2000GL012243, 2001

Kawahata, H., Fujita, K., Iguchi, A., Inoue, M., Iwasaki, S., Kuroyanagi, A., Maeda, A., Manaka, T., Moriya, K., Takagi, H., Toyofuku, T., Yoshimura, T., and Suzuki, A.: Perspective on the response of marine calcifiers to global warming and ocean acidification – Behavior of corals and foraminifera in a high CO_2 world hot house, Progress Earth Planet. Sci., 6, 5, https://doi.org/10.1186/s40645-018-0239-9, 2019.

Kim, S.: Seismic stratigraphy and tomography in the northwestern Ross Sea outer margin: implications for late Cenozoic Antarctic ice-sheet evolution and bottom-current activity, PhD thesis, University of Science and Technology, Daejeon, Republic of Korea, 117 pp., 2018.

Kim, S., Lee, J. I., McKay, R. M., Yoo, K.-C., Bak, Y.-S., Lee, M. K., Roh, Y. H., Yoon, H. I., Moon, H. S., and Hyun, C.-U.: Late pleistocene paleoceanographic changes in the Ross Sea e Glacial-interglacial variations in paleoproductivity, nutrient utilization, and deep-water formation, Quaternary Sci. Rev., 239, 106356, https://doi.org/10.1016/j.quascirev.2020.106356, 2020.

Leventer, A.: Sediment trap diatom assemblages from the northern Antarctic Peninsula region, Deep-Sea Res., 38, 1127–1143, https://doi.org/10.1016/0198-0149(91)90099-2, 1991.

Licht, K. J., Jennings, A. E., Andrews, J. T., and Williams, K. M.: Chronology of late Wisconsin ice retreat from the western Ross Sea, Antarctica, Geology, 24, 223–226, https://doi.org/10.1130/0091-7613(1996)024<0223:COLWIR>2.3.CO;2, 1996.

Lipps, J. H. and Krebbs, W. N.: Planktonic Foraminifera associated with Antarctic sea ice, J. Foram. Res., 4, 80–85, https://doi.org/10.2113/gsjfr.4.2.80, 1974.

Livingstone, S. J., Cofaigh, C. Ó., Stokes, C. R., Hillenbrand, C.-D., Vieli, A., and Jamieson, S. S. R.: Antarctic palaeo-ice streams, Earth-Sci. Rev., 111, 90–128, https://doi.org/10.1016/j.earscirev.2011.10.003, 2012.

Lowry, D. P., Golledge, N. R., Bertler, N. A. N., Jones, R. S., and McKay, R.: Deglacial grounding-line retreat in the Ross Embayment, Antarctica, controlled by ocean and atmosphere forcing, Sci. Adv., 5, eaav8754, https://doi.org/10.1126/sciadv.aav8754, 2019.

Lynch-Stieglitz, J., Stocker, T. F., Broecker, W. S., and Fairbanks, R. G.: The influence of air-sea exchange on the isotopic composition of oceanic carbon: Observations and modeling, Global Biogeochem. Cy., 9, 653–665, https://doi.org/10.1029/95GB02574, 1995.

Maas, S. M.: Last Glacial Maximum – Holocene glacial and depositional history from sediment cores at Coulman High beneath the Ross Ice Shelf, Antarctica, Master thesis, Victoria University of Wellington, Wellington, New Zealand, 114 pp., 2012.

Mackensen, A., Grobe, H., Kuhn, G., and Fütterer, D. K.: Benthic foraminiferal assemblages from the eastern Weddell Sea between 68 and 73° S: distribution, ecology and fossilization potential, Mar. Micropaleontol., 16, 241–283, https://doi.org/10.1016/0377-8398(90)90006-8, 1990.

Mackensen, A., Futterer, D. K., Grobe, H., and Schmiedl, G.: Benthic foraminiferal assemblages from the eastern South Atlantic Polar Front region between 35 and 57 S: Distribution, ecology and fossilization potential, Mar. Micropaleontol., 22, 33–69, https://doi.org/10.1016/0377-8398(93)90003-G, 1993.

Mackensen, A., Grobe, H., Hubberten, H. W., and Kuhn, G.: Benthic foraminiferal assemblages and the δ^{13}C-signal in the Atlantic sector of the Southern Ocean: Glacial-to-interglacial contrasts, in: Carbon cycling in the glacial ocean: Constraints on the ocean's role in global change, edited by: Zahn, R., Kaminski, M., Labeyrie, L., and Pedersen, T., Springer, Berlin, Germany, 105–144, 1994.

Mackintosh, A. N., Verleyen, E., O'Brien, P. E., White, D. A., Jones, R. S., McKay, R., Dunbar, R., Gore, D. B., Fink, D., Post, A. L., Miura, H., Leventer, A., Goodwin, I., Hodgson, D. A., Lilly, K., Crosta, X., Golledge, N. R., Wagner, B., Berg, S., van Ommen, T., Zwartz, D., Roberts, S. J., Vyverman, W., and Masse, G.: Retreat history of the East Antarctic Ice Sheet since the Last Glacial Maximum, Quaternary Sci. Rev., 100, 10–30, https://doi.org/10.1016/j.quascirev.2013.07.024, 2014.

Maddison, E. J., Pike, J., Leventer, A., and Domack, E. W.: Deglaciation seasonal and sub-seasonal diatom record from Palmer Deep, Antarctica, J. Quatern. Sci., 20, 435–446, https://doi.org/10.1002/jqs.947, 2005.

Majewski, W.: Benthic foraminiferal communities: distribution and ecology in Admiralty Bay, King George Island, West Antarctica, Pol. Polar Res., 26, 159–214, 2005.

Majewski, W. and Pawlowski, J.: Morphologic and molecular diversity of the foraminiferal genus *Globocassidulina* in Admiralty Bay, King George Island, Antarct. Sci., 22, 271–281, https://doi.org/10.1017/S0954102010000106, 2010.

Majewski, W., Wellner, J. S., and Anderson, J. B.: Environmental connotations of benthic foraminiferal assemblages from coastal West Antarctica, Mar. Micropaleontol., 124, 1–15, https://doi.org/10.1016/j.marmicro.2016.01.002, 2016.

Majewski, W., Bart, P. J., and McGlannan, A. J.: Foraminiferal assemblages from ice-proximal paleo-settings in the Whales Deep Basin, Eastern Ross Sea, Antarctica, Palaeogeogr. Palaeocl., 493, 64–81, https://doi.org/10.1016/j.palaeo.2017.12.041, 2018.

Majewski, W., Prothro, L. O., Simkins, L. M., Demianiuk, E. J., and Anderson, J. B.: Foraminiferal patterns in deglacial sediment in the western Ross Sea, Antarctica: life near grounding lines, Paleoceanogr. Paleocl., 35, e2019PA003716, https://doi.org/10.1029/2019PA003716, 2020.

Malinverno, E.: Extant morphotypes of *Distephanus speculum* (Silicoflagellata) from the Australian sector of the Southern Ocean: Morphology, morphometry and biogeography, Mar. Micropaleontol., 77, 154–174, https://doi.org/10.1016/j.marmicro.2010.09.002, 2010.

Malinverno, E., Maffioli, P., and Gariboldi, K.: Latitudinal distribution of extant fossilizable phytoplankton in the Southern Ocean: Planktonic provinces, hydrographic fronts and

palaeoecological perspectives, Mar. Micropaleontol., 123, 41–58, https://doi.org/10.1016/j.marmicro.2016.01.001, 2016.

Masson, V., Vimeux, F., Jouzel, J., Morgan, V., Delmotte, M., Cias, P., Hammer, C., Johnsen, S., Lipenkov, V. Y., Mosley-Thompson, E., Petit, J., Steig, E. J., Stievenard, M., and Vaikmae, R.: Holocene climate variability in Antarctica based on 11 ice-core isotopic records, Quatern. Res., 54, 348–358, https://doi.org/10.1006/qres.2000.2172, 2000.

McCave, I. N., Manighetti, B., and Robinson, S. G.: Sortable silt and fine sediment size/composition slicing: Parameters for palaeocurrent speed and palaeoceanography, Paleoceanogr. Paleocl., 10, 593–610, https://doi.org/10.1029/94PA03039, 1995.

McGlannan, A. J., Bart, P. J., Chow, J. M., and DeCesare, M.: On the influence of post-LGM ice shelf loss and grounding zone sedimentation on West Antarctic ice sheet stability, Mar. Geol., 392, 151–169, https://doi.org/10.1016/j.margeo.2017.08.005, 2017.

Melis, R. and Salvi, G.: Late Quaternary foraminiferal assemblages from western Ross Sea (Antarctica) in relation to the main glacial and marine lithofacies, Mar. Micropaleontol., 70, 39–53, https://doi.org/10.1016/j.marmicro.2008.10.003, 2009.

Melis, R. and Salvi, G.: Foraminifer and Ostracod Occurrence in a Cool-Water Carbonate Factory of the Cape Adare (Ross Sea, Antarctica): A Key Lecture for the Climatic and Oceanographic Variations in the Last 30,000 Years, Geosciences, 10, 413, https://doi.org/10.3390/geosciences10100413, 2020.

Melis, R., Colizza, E., Pizzolato, F., and Rosso, A.: Preliminary study of the calcareous taphocoenoses in Late Quaternary glacial marine sequences of the Ross Sea (Antarctica), Geobios, 35, 207–218, https://doi.org/10.1016/S0016-6995(02)00060-8, 2002.

Mezgec, K.: Palaeoceanographic changes during the post-LGM deglaciation phase in the polar areas (Ross Sea-Antarctica and Barents Sea-Arctic cases studies), PhD Thesis, University of Siena, Siena, Italy, 156 pp., 2015.

Mezgec, K., Stenni, B., Crosta, X., Masson-Delmotte, V., Baroni, C., Braida, M., Ciardini, V., Colizza, E., Melis, R., Salvatore, M. C., Severi, M., Scarchilli, C., Traversi, R., Udisti, R., and Frezzotti, M.: Holocene sea ice variability driven by wind and polynya efficiency in the Ross Sea, Nat. Commun., 8, 1334, https://doi.org/10.1038/s41467-017-01455-x, 2017.

Mikis, A., Hendry, K. R., Pike, J., Schmidt, D. N., Edgar, K. M., Peck, V., Peeters, F. J. C., Leng, M. J., Meredith, M. P., Todd, C. L., Stammerjohn, S., and Ducklow, H.: Temporal variability in foraminiferal morphology and geochemistry at the West Antarctic Peninsula: a sediment trap study, Biogeosciences, 16, 3267–3282, https://doi.org/10.5194/bg-16-3267-2019, 2019.

Minzoni, R. T., Anderson, J. B., Fernandez, R., and Wellner, J. S.: Marine record of Holocene climate, ocean, and cryosphere interactions: Herbert Sound, James Ross Island, Antarctica, Quaternary Sci. Rev., 129, 239–259, https://doi.org/10.1016/j.quascirev.2015.09.009, 2015.

Murray, J. W. and Pudsey, C. J.: Living (stained) and dead foraminifera from the newly ice-free Larsen Ice Shelf, Weddell Sea, Antarctica: ecology and taphonomy, Mar. Micropaleontol., 53, 67–81, https://doi.org/10.1016/j.marmicro.2004.04.001, 2004.

Nair, A., Mohan, R., Manoj, M. C., and Thamban, M.: Glacial-interglacial variability in diatom abundance and valve size: Implications for Southern Ocean paleoceanography, Paleoceanogr. Paleocl., 30, 1245–1260, https://doi.org/10.1002/2014PA002680, 2015.

Pike, J., Allen, C. S., Leventer, A., Stickley, C. E., and Pudsey, C. J.: Comparison of contemporary and fossil diatom assemblages from the western Antarctic Peninsula shelf, Mar. Micropaleontol., 67, 274–287, https://doi.org/10.1016/j.marmicro.2008.02.001, 2008.

Pike, J., Crosta, X., Maddison, E. J., Stickley, C. E., Denis, D., Barbara, L., and Renssen, H.: Observations on the relationship between the Antarctic coastal diatoms *Thalassiosira antarctica* Comber and *Porosira glacialis* (Grunow) Jørgensen and sea ice concentrations during the late Quaternary, Mar. Micropaleontol., 73, 14–25, https://doi.org/10.1016/j.marmicro.2009.06.005, 2009.

Pike, J., Swann, G. E. A., Leng, M. J., and Snelling, A. M.: Glacial discharge along the west Antarctic Peninsula during the Holocene, Nat. Geosci., 6, 199–202, https://doi.org/10.1038/ngeo1703, 2013.

Prothro, L. O., Simkins, L. M., Majewski, W., and Anderson, J. B.: Glacial retreat patterns and processes determined from integrated sedimentology and geomorphology records, Mar. Geol., 395, 104–119, https://doi.org/10.1016/j.margeo.2017.09.012, 2018.

Prothro, L. O., Majewski, W., Yokoyama, Y., Simkins, L. M., Anderson, J. B., Yamane, M., Miyairi, Y., and Ohkouchi, N.: Timing and pathways of East Antarctic Ice Sheet retreat, Quaternary Sci. Rev., 230, 106166, https://doi.org/10.1016/j.quascirev.2020.106166, 2020.

Pudsey, C. J., Murray, J. W., Appleby, P., and Evans, J.: Ice shelf history from petrographic and foraminiferal evidence, northeast Antarctic Peninsula, Quaternary Sci. Rev., 25, 2357–2379, https://doi.org/10.1016/j.quascirev.2006.01.029, 2006.

Quaia, T. and Cespuglio, G.: Oxygen and carbon stable isotopes in foraminifers from cores ANTA91-8 and ANTA91-2 (Ross Sea), Museo Nazionale dell'Antartide, Italy, Terra Ant. Rep., 4, 199–210, 2000.

Rathburn, A. E., Pichon, J. J., Ayress, M. A., and De Deckker, P.: Microfossil and stable-isotope evidence for changes in Late Holocene palaeoproductivity and palaeoceanographic conditions in the Prydz Bay region of Antarctica, Palaeogeogr. Palaeocl., 131, 485–510, https://doi.org/10.1016/S0031-0182(97)00017-5, 1997.

Reimer, P. J., Bard, E., Bayliss, A., Beck, J. W., Blackwell, P. G., Bronk Ramsey, C., Buck, C. E., Edwards, R. L., Friedrich, M., Grootes, P. M., Guilderson, T. P., Haflidason, H., Hajdas, I., Hatté, C., Heaton, T. J., Hoffmann, D. L., Hogg, A. G., Hughen, K. A., Kaiser, K. F., Kromer, B., Manning, S. W., Niu, M., Reimer, R. W., Richards, D. A., Scott, E. M., Southon, J. R., Turney, C. S. M., and van der Plicht, J.: IntCal13 and Marine13 radiocarbon age calibration curves, 0–50,000 years cal BP, Radiocarbon, 55, 1869–1887, https://doi.org/10.2458/azu_js_rc.55.16947, 2013.

Rigual-Hernández, A. S., Trull, T. W., Bray, S. G., Cortina, A., and Armand, L. K.: Latitudinal and temporal distributions of diatom populations in the pelagic waters of the Subantarctic and Polar Frontal zones of the Southern Ocean and their role in the biological pump, Biogeosciences, 12, 5309–5337, https://doi.org/10.5194/bg-12-5309-2015, 2015.

Salvi, C., Salvi, G., Stenni, B., and Brambati, A.: Palaeoproductivity in the Ross Sea, Antarctica, during the last 15 kyr BP and its link

with ice-core temperature proxies, Ann. Glaciol., 39, 445–451, https://doi.org/10.3189/172756404781814582, 2004.

Schmiedl, G., Mackensen, A., and Mueller, P. J.: Recent benthic foraminifera from the eastern South Atlantic Ocean: dependence on food supply and water masses, Mar. Micropaleontol., 32, 249–287, https://doi.org/10.1016/S0377-8398(97)00023-6, 1997.

Shewenell, A. E., Ingalls, A., and Domack, E.: Holocene Southern Ocean surface temperature variability west of the Antarctic Peninsula, Nature, 470, 250–254, https://doi.org/10.1038/nature09751, 2011.

Shipp, S. S., Anderson, J. B., and Domack, E. W.: Late Pleistocene – Holocene retreat of the West Antarctic Ice-Sheet system in the Ross Sea: Part 1 – Geophysical results, Geol. Soc. Am. Bull., 111, 1486–1516, https://doi.org/10.1130/0016-7606(1999)111<1486:LPHROT>2.3.CO;2, 1999.

Shipp, S. S., Wellner, J. S., and Anderson, J. B.: Retreat signature of a polar ice stream: sub-glacial geomorphic features and sediments from the Ross Sea, Antarctica, in: Glacier-influenced Sedimentation on High Latitude Continental Margins, edited by: Dowdeswell, J. A. and O'Cofaigh, C., Geological Society of London, London, UK, 277–304, https://doi.org/10.1144/GSL.SP.2002.203.01.15, 2002.

Simkins, L. M., Anderson, J. B., Greenwood, S. L., Gonnermann, H. M., Prothro, L. O., Halberstadt, A. R. W., Stearns, L. A., Pollard, D., and DeConto, R. M.: Anatomy of a meltwater drainage system beneath the ancestral East Antarctic ice sheet, Nat. Geosci., 10, 691–697, https://doi.org/10.1038/ngeo3012, 2017.

Sjunneskog, C. and Scherer, R.: Mixed diatom assemblages in glacigenic sediment from the Central Ross Sea, Antarctica, Palaeogeogr. Palaeocl., 218, 287–300, https://doi.org/10.1016/j.palaeo.2004.12.019, 2005.

Smith, J. A., Hillenbrand, C.-D., Pudsey, C. J., Allen, C. S., and Graham, A. G. C.: The presence of polynyas in the Weddell Sea during the Last Glacial Period with implications for the reconstruction of sea-ice limits and ice sheet history, Earth Planet. Sc. Lett., 296, 287–298, https://doi.org/10.1016/j.epsl.2010.05.008, 2010.

Smith, J. A., Graham, A. G. C., Post, A. L., Hillebrand, C.-D., Bart, P. J., and Powell, R. D.: The marine geological imprint of Antarctic ice shelves, Nat. Commun., 10, 5635, https://doi.org/10.1038/s41467-019-13496-5, 2019.

Smith Jr., W. O., Sedwick, P. N., Arrigo, K. R., Ainley, D. G., and Orsi, A. H.: The Ross Sea in a sea of change, Oceanography, 25, 90–103, https://doi.org/10.5670/oceanog.2012.80, 2012.

Spindler, M. and Dieckmann, G. S.: Distribution and abundance of the planktic foraminifer *N. pachyderma* in the sea ice of the Weddell Sea (Antarctica), Polar Biol., 5, 185–191, https://doi.org/10.1007/BF00441699, 1986.

Stevens, C., Hulbe, C., Brewer, M., Stewart, C., Robinson, N., Ohneiser, C., and Jendersie, S.: Ocean mixing and heat transport processes observed under the Ross Ice Shelf control its basal melting, P. Natl. Acad. Sci. USA, 117, 16799–16804, https://doi.org/10.1073/pnas.1910760117, 2020.

Taylor, F. and Sjunneskog, C.: Postglacial marine diatom record of the Palmer Deep, Antarctic Peninsula (ODP Leg 178, Site 1098) 2. Diatom assemblages, Paleoceanogr. Paleocl., 17, 8001, https://doi.org/10.1029/2000PA000564, 2002.

Taylor, F., Whitehead, J., and Domack, E.: Holocene paleoclimate change in the Antarctic Peninsula: evidence from the diatom, sedimentary and geochemical record, Mar. Micropaleontol., 41, 25–43, https://doi.org/10.1016/S0377-8398(00)00049-9, 2001.

Tesi, T., Belt, S. T., Gariboldi, K., Muschitiello, F., Smik, L., Finocchiaro, F., Giglio, F., Colizza, E., Gazzurra, G., Giordano, P., Morigi, C., Capotondi, L., Nogarotto, A., Köseoğlu, D., Di Roberto, A., Gallerani, A., and Langone, L.: Resolving sea ice dynamics in the north-western Ross Sea during the last 2.6 ka: From season to millennial timescales, Quaternary Sci. Rev., 237, 106299, https://doi.org/10.1016/j.quascirev.2020.106299, 2020.

Thomas, E., Booth, L., Maslin, M., and Shackleton, N. J.: Northeastern Atlantic benthic foraminifera during the last 45,000 years: Changes in productivity seen from the bottom up, Paleoceanogr. Paleocl., 10, 545–562, https://doi.org/10.1029/94PA03056, 1995.

Thomas, E. R., Allen, C. S., Etourneau, J., King, A. C. F., Severi, M., Winton, V. H. L., Mueller, J., Crosta, X., and Peck, V. L.: Antarctic Sea Ice Proxies from Marine and Ice Core Archives Suitable for Reconstructing Sea Ice over the Past 2000 Years, Geosciences, 9, 506, https://doi.org/10.3390/geosciences9120506, 2019.

Tinto, K. J., Padman, L., Siddoway, C. S., Springer, S. R., Fricker, H. A., Das, I., Caratori Tontini, F., Porter, D. F., Frearson, N. P., Howard, S. L., Siegfried, M. R., Mosbeux, C., Becker, M. K., Bertinato, C., Boghosian, A., Brady, N., Burton, B. L., Chu, W., Cordero, S. I., Dhakal, T., Dong, L., Gustafson, C. D., Keeshin, S., Locke, C., Lockett, A., O'Brien, G., Spergel, J. J., Starke, S. E., Tankersley, M., Wearing, M. G., and Bell, R. E.: Ross Ice Shelf response to climate driven by the tectonic imprint on seafloor bathymetry, Nat. Geosci., 12, 441–449, https://doi.org/10.1038/s41561-019-0370-2, 2019.

Tolotti, R., Salvi, C., Salvi, G., and Bonci, M. C.: Late Quaternary climate variability as recorded by micropaleontological diatom data and geochemical data in the Western Ross Sea, Antarctica, Antarct. Sci., 25, 804–820, https://doi.org/10.1017/S0954102013000199, 2013.

Violanti, D.: Taxonomy and distribution of recent benthic foraminifers from Terra Nova Bay (Ross Sea, Antarctica), Oceanographic Campaign 1987/1988, Palaeontogr. Ital., 83, 25–71, 1996.

Wacker, L., Lippold, J., Molnár, M., and Schulz, H.: Towards radiocarbon dating of single foraminifera with a gas ion source, Nucl. Instrum. Meth. B, 294, 307–310, https://doi.org/10.1016/j.nimb.2012.08.038, 2013.

Wollenburg, J. and Mackensen, A.: Modern benthic foraminifera from the central Arctic Ocean: faunal composition, standing stock, and diversity, Mar. Micropaleontol., 34, 153–185, 1998.

Wollenburg, J. E. and Kuhnt, W.: The response of benthic foraminifers to carbon flux and primary production in the Arctic Ocean, Mar. Micropaleontol., 40, 189–231, https://doi.org/10.1016/S0377-8398(00)00039-6, 2000.

Xiao, W., Esper, O., and Gersonde, R.: Last Glacial-Holocene climate variability in the Atlantic sector of the Southern Ocean, Quaternary Sci. Rev., 135, 115–137, https://doi.org/10.1016/j.quascirev.2016.01.023, 2016.

Yokoyama, Y., Esat, T. M., Thompson, W. G., Thomas, A. L., Webster, S. M., Miyairi, Y., Sawada, C., Aze, T., Matsuzaki, H., Okuno, J. I., and Fallon, S.: Rapid glaciations and a two-step sea level plunge into the Last Glacial Maximum, Nature, 599, 603–607, https://doi.org/10.1038/s41586-018-0335-4, 2018.